The ELF3-BBX24/BBX25-PIF4 module controls thermosensory growth in Arabidopsis

Bidhan Chandra Malakar[1], Shivani Singh[1], Vikas Garhwal[1,#], Rajanesh Chandramohan[1,#], Gouranga Upadhyaya[1], and Sreeramaiah N. Gangappa[1,2,*]

Affiliations:

[1]Department of Biological Sciences, Indian Institute of Science Education and Research Kolkata, Mohanpur 741246, West Bengal, India

[2]Centre for Climate and Environmental Studies, Indian Institute of Science Education and Research Kolkata, Mohanpur 741246, West Bengal, India

*Author for correspondence: ngsreeram@iiserkol.ac.in (S.N.G)

[#]Authors contributed equally

The author responsible for the distribution of data and materials integral to the findings presented in this article as per the policy described in the Instructions for Authors is Sreeramaiah N. Gangappa (ngsreeram@iiserkol.ac.in)

ABSTRACT

Temperature serves as a crucial environmental cue governing the growth and adaptation of plants in their natural habitat. PHYTOCHROME INTERACTING FACTOR 4 (PIF4) is a central regulator that promotes thermomorphogenesis in Arabidopsis. Understanding its precise regulation is critical for optimal thermomorphogenic growth. Here, we identified two BBX proteins, BBX24 and BBX25, as novel components of the PIF4-mediated thermosensory pathway and act to promote warm temperature-mediated growth. The *bbx24* and *bbx25* single and double mutants showed moderate to strong temperature-insensitive hypocotyl and cotyledon growth. Warm temperature induces *BBX24* and *BBX25* mRNA expression and protein accumulation. Genetic and biochemical analysis revealed that BBX24/BBX25 promotes PIF4-mediated thermosensory growth by counteracting a key component of the evening complex, ELF3. While ELF3 inhibits *BBX24*/*BBX25* gene expression at low ambient temperatures in the evening, warm temperature-mediated inhibition of ELF3 activity results in enhanced BBX24/BBX25 activity. Moreover, BBX24/25 inhibit ELF3 function through direct physical interaction and likely relieves repression on PIF4, enhancing its activity and thermomorphogenesis. Together, this study unravels ELF3-BBX24/BBX25-PIF4 as a key regulatory module that controls growth and development under varying temperature cues.

Keywords: Thermomorphogenesis, BBX24, BBX25, PIF4, ELF3, gene regulation

INTRODUCTION

69 Ecological cues such as light and temperature are key in regulating plant growth,
70 architecture, and fitness (Casal and Balasubramanian, 2019; Casal and Questa,
71 2018; Franklin et al., 2014; Legris et al., 2019; Lippmann et al., 2019; Quint et al.,
72 2023). Plants have evolved sophisticated and multifaceted mechanisms to perceive,
73 integrate, and process these cues (Krahmer and Fankhauser, 2023; Legris *et al.*,
74 2019). Because plants experience these conflicting signals, they must constantly
75 sense and integrate them to optimise growth and acclimate to local environments.
76 Warm ambient temperatures strongly influence plant growth by accelerating
77 vegetative and reproductive transitions, resulting in shortened life-cycle duration
78 (Casal and Balasubramanian, 2019; Crawford et al., 2012; Koini et al., 2009;
79 Krahmer and Fankhauser, 2023; Kumar et al., 2012; Quint *et al.*, 2023). However,
80 warm temperatures strongly compromise immunity and severely affect seed set and
81 yield (Burroughs et al., 2023; Koester et al., 2014; Zhao et al., 2017). Increasing
82 seasonal growth temperature due to global warming impairs plant growth and yield,
83 threatening farmers' livelihood and food security (Peng et al., 2004; Zhao *et al.*,
84 2017). Therefore, understanding how plants sense and integrate temperature cues
85 is critical to delineating thermosensory signalling mechanisms to breed climate-
86 resilient crops.

87 The light signaling pathway consists of photoreceptors and downstream signaling
88 molecules that have been shown to play a pivotal role in sensing and integrating
89 temperature cues (Legris *et al.*, 2019; Li et al., 2016). Key studies revealed that red-
90 light absorbing phytochrome B (phyB) senses temperature cues (Jung et al., 2016;
91 Legris et al., 2016). PhyB exists in two interconvertible physiologically active (Pfr)
92 and inactive (Pr) forms. Warm temperature favours the conversion of Pfr to Pr form,
93 reducing the phyB activity (Legris *et al.*, 2016). The phyB targets a group of growth-
94 promoting transcription factors, PHYTOCHROME INTERACTING FACTORS
95 (PIFs), for phosphorylation and degradation in a red-light-dependent manner (de
96 Lucas et al., 2008; Huq and Quail, 2002; Lorrain et al., 2008). Among PIFs, PIF4
97 and PIF7 have been shown to mediate thermomorphogenesis, respectively, under
98 SD and LD photoperiods (Burko et al., 2022; Chung et al., 2020; Delker et al., 2022;
99 Fiorucci et al., 2020; Koini *et al.*, 2009; Kumar *et al.*, 2012). PIF4 is essential for

100 warm temperature-induced hypocotyl and petiole growth, rosette development,
101 hyponasty, and flowering (Casal and Balasubramanian, 2019; Favero et al., 2020;
102 Koini *et al.*, 2009; Kumar *et al.*, 2012; Oh et al., 2012; Quint *et al.*, 2023; Quint et al.,
103 2016; Zhao and Bao, 2021). PIF4-mediated thermomorphogenesis is linked to the
104 activation of genes involved in auxin/brassinosteroid biosynthesis and signaling
105 (Franklin et al., 2011; Ibanez et al., 2018; Krahmer and Fankhauser, 2023; Sun et
106 al., 2012), cell elongation (Gangappa and Kumar, 2017) and flowering(Kumar *et al.*,
107 2012). Warm temperature-mediated inhibition of phyB activity increases PIF4
108 function, resulting in thermosensory growth (Legris *et al.*, 2016). Unlike phyB, the
109 blue light receptor Cryptochrome 1 (CRY1) inhibits thermomorphogenesis through
110 PIF4 sequestration(Ma et al., 2016). The central oscillator components of the
111 circadian clock, including the evening complex (EC), play a crucial role in controlling
112 thermomorphogenesis by regulating PIF4 function. The EARLY FLOWERING 3
113 (ELF3), a critical component of the evening complex (EC) and a thermosensor,
114 inhibits *PIF4* transcription and also sequesters it by forming heterodimers (Box et al.,
115 2015; Jung et al., 2020; Nieto et al., 2015; Nusinow et al., 2011). Moreover, upstream
116 regulatory components such as CONSTITUTIVE PHOTOMORPHOGENIC 1
117 (COP1), DE-ETIOLATED 1 (DET1) and SUPPRESSOR OF PHYTOCHROME A-
118 105 1 (SPA1) proteins promote PIF4-mediated thermomorphogenic growth by
119 stabilizing PIF4 protein (Gangappa and Kumar, 2017; Lee et al., 2020; Park et al.,
120 2017). Recent studies also reveal that the HEMERA/REGULATOR OF the
121 CHLOROPLAST BIOGENESIS (HMR/RCB) module works cooperatively to stabilize
122 PIF4 during the day and promote thermomorphogenesis (Qiu et al., 2019; Qiu et al.,
123 2021). The Heat shock transcription factor (HSF) family members, HSFA1a/b/d/e,
124 interact with PIF4 and stabilize it during light by interfering with PIF4-phyB
125 interaction, resulting in thermomorphogenesis during the day (Tan et al., 2023a).

126 The B-BOX containing zinc-finger (BBX) proteins are highly conserved transcription
127 factors across eukaryotes that regulate gene expression by directly binding to DNA
128 or as transcriptional co-activators or co-repressors through protein-protein
129 interaction. BBX proteins have emerged as crucial integrators of various
130 environmental cues (Ding et al., 2018; Gangappa and Botto, 2014; Khanna et al.,

131 2009; Song et al., 2020; Vaishak et al., 2019; Yuan et al., 2021). The BBX24 and
132 BBX25 are close homologs that function as transcriptional co-repressors of HY5 to
133 inhibit photomorphogenesis (Gangappa et al., 2013; Job et al., 2018). Additionally,
134 BBX24 functions in various signaling pathways, including UV-B signaling (Huang et
135 al., 2022; Jiang et al., 2012), shade-avoidance response (Crocco et al., 2015; Saura-
136 Sanchez et al., 2023) and flowering (Li et al., 2014). However, the role of BBX24 and
137 BBX25 in temperature-mediated regulation of growth and development remains
138 unknown. Here, we report that BBX24/BBX25 as key regulators of PIF4-mediated
139 thermosensory growth. We found that *BBX24*/*BBX25* gene expression and protein
140 levels are enhanced at warm temperatures, further enhancing PIF4 protein
141 accumulation and thermomorphogenesis. Our study demonstrates that ELF3
142 functions upstream of BBX24/BBX25, inhibiting their gene expression during the
143 evening hours under low temperatures. However, warm temperature-mediated
144 inhibition of ELF3 activity results in increased BBX24/BBX25 function and, in turn,
145 enhances PIF4-mediated thermomorphogenic growth. Additionally, BBX24/BBX25
146 inhibit ELF3 protein accumulation resulting in the release of the negative inhibitory
147 effect of ELF3 on PIF4 protein and transcript accumulation. Together, this study
148 uncovers a novel regulatory mechanism by which BBX24/BBX25 promote PIF4-
149 mediated thermosensory growth via antagonizing ELF3 function.

150

151 ## RESULTS

152

153 **BBX24 and BBX25 are essential for warm temperature-mediated growth**

154 To unravel the possible role of BBX24 and BBX25 in temperature-mediated
155 regulation of hypocotyl growth, we analyzed the hypocotyl growth response of wild-
156 type (Col-0) and *bbx24* and *bbx25* mutants grown under 22°C and 27°C. Our data
157 revealed that *bbx24* and *bbx25* had moderate but significantly shorter hypocotyls at
158 22°C and 27°C than Col-0 both under short-day (SD) and long-day (LD)
159 photoperiods (Figure 1A-1C). Compared to Col-0, *bbx24* showed stronger inhibition
160 in hypocotyl growth than the *bbx25* mutant at 27°C (Figure 1A-1C). Interestingly, the
161 *bbx24bbx25* double mutant had a much shorter hypocotyl length at 27°C than the

162 single mutants (Figure 1A-1C), suggesting their additive function in promoting warm
163 temperature-mediated hypocotyl growth. Contrary to mutants, the *BBX24*
164 overexpression (hereafter referred to as *BBX24-OE*) transgenic line showed
165 enhanced thermosensory hypocotyl growth as they had significantly longer
166 hypocotyls than Col-0 at 22°C and 27°C both under SD and LD (Figure 1D-1F). To
167 further understand whether overexpression of *BBX25* has a similar effect to *BBX24-*
168 *OE* in promoting hypocotyl growth, we generated multiple transgenic lines
169 overexpressing *BBX25* (Supplemental Figure S1A and 1B). Like *BBX24-OE* lines,
170 transgenic lines overexpressing *BBX25* showed exaggerated hypocotyl growth
171 compared to Col-0 at 22°C and 27°C, under SD and LD (Figure 1D-1F;
172 Supplemental Figure S1C-S1E). Warm temperature-mediated hypocotyl elongation
173 is attributed to increased cell elongation, which is due to increased growth-promoting
174 hormones such as auxin and brassinosteroid (Franklin *et al.*, 2011; Ibanez *et al.*,
175 2018; Oh *et al.*, 2012). To know if BBX24/BBX25-mediated hypocotyl growth is due
176 to increased cell elongation, we analyzed the cell length of hypocotyl epidermal cells
177 from seedlings grown at 22°C and 27°C under SD. Our data reveal that the hypocotyl
178 epidermal cell length was significantly longer in Col-0 at 27°C than at 22°C (Figure
179 1G). However, in the *bbx24bbx25* double mutant, the cell length was strongly
180 inhibited (Figure 1G). Contrarily, *BBX24* and *BBX25* overexpression lines had
181 significantly longer cells at both 22°C and 27°C than Col-0 (Figure 1G). Together,
182 these results suggest that BBX24/BBX25-mediated hypocotyl growth in response to
183 warm temperature is linked to an increase in cell elongation of hypocotyl epidermal
184 cells.

185 Warm temperature-mediated hypocotyl growth is linked to enhanced accumulation
186 of auxin and brassinosteroid (BR) growth hormones (Franklin *et al.*, 2011; Gray et
187 al., 1998; Ibanez *et al.*, 2018; Krahmer and Fankhauser, 2023; Oh *et al.*, 2012;
188 Stavang et al., 2009). As *bbx24bbx25* double mutant has extremely short hypocotyls
189 under warm temperatures, we wanted to see if exogenous application of auxin or BR
190 can rescue this phenotype. Our data suggest that in response to a synthetic auxin
191 picloram (PIC) or epibrassinolide (eBL) the short hypocotyl phenotype of
192 *bbx24bbx25* was partially recovered with a higher % hypocotyl growth at 27°C

193 compared to Col-0 (Supplemental Figure S2A-F). In contrast, *BBX24-OE* and
194 *BBX25-OE* lines showed enhanced sensitivity to both the hormones with a reduced
195 % hypocotyl growth compared to Col-0 (Supplemental Figure S2A-F). Moreover, we
196 also found that overexpression of *BBX24* and *BBX25* enhanced the promoter activity
197 of *DR5*, a synthetic auxin reporter (Supplemental Figure S2G). Contrastingly, when
198 we treated the *BBX24-OE* and *BBX25-OE* seedlings with auxin inhibitor 2,3,5-
199 triiodobenzoic acid (TIBA, an auxin transport inhibitor) and a BR biosynthetic
200 inhibitor, Propiconazole (PPZ), they showed enhanced sensitivity to the inhibitor
201 similar to Col-0 (Supplemental Figure S3A-F). Thus, these results suggest that
202 BBX24/BBX25 indeed promote auxin/BR governed hypocotyl growth in response to
203 warmth.

204 **BBX24/BBX25 function is necessary for the thermoresponsive gene**
205 **expression**

206 Consistent with the hypocotyl data, our qRT-PCR results from SD-grown seedlings
207 harvested at ZT23 revealed that auxin biosynthetic gene *YUCCA8* (*YUC8*), cell-wall
208 elongation gene *XYLOGLUCAN ENDOTRANSGLYCOSYLASE 7* (*XTR7*), auxin
209 signaling gene *INDOLE ACETIC ACID19* (*IAA19*), BR signaling gene
210 *PACLOBUTRAZOL RESISTANCE5* (*PRE5*) showed significant downregulation in
211 the *bbx24bbx25* mutant at 27°C, while moderately reduced at 22°C, compared to
212 Col-0 (Figure 1H). However, in the *BBX24* and *BBX25* overexpression lines, these
213 genes showed significant upregulation both at 22°C and 27°C (Figure 1H).
214 Additionally, our qPCR data from SD-grown seedlings harvested during daytime at
215 ZT3 revealed that expression of growth and hormone signaling genes such as
216 *YUC8*, *DWARF4* (*DWF4*), *Gibberellin 3-oxidases* (*GA3OX1*), *IAA19*, *PRE5*,
217 *SMALL* AUXIN *UP-REGULATED RNA 21* (*SAUR21*), and genes involved in cell
218 elongation, such as *EXPANSIN 8* (*EXP8*) and *XTR7* showed significant
219 downregulation in the *bbx24bbx25* double mutant while upregulated in the
220 overexpression lines than Col-0, at 22°C and 27°C (Supplemental Figure S4A and
221 B). Together, these data confirm that BBX24/BBX25 induce the expression of

222 growth-related genes in response to warm temperatures both at night and during the
223 day.

224 **BBX24/BBX25 gene expression and protein levels are enhanced in response**
225 **to warm temperatures**

226 As BBX24/BBX25 promote warm temperature-mediated hypocotyl growth, we
227 wanted to see if warm temperature regulates their gene expression and protein
228 abundance. The qRT-PCR data from six-day-old seedlings revealed that *BBX24* and
229 *BBX25* transcript levels showed significant upregulation at 27°C compared to 22°C
230 both at the end of the night (ZT23) and during daytime (ZT3) (Supplemental Figure
231 S5A). Further, when we monitored the expression of *BBX24* and *BBX25* for an
232 extended period during the day into early night, we found that *BBX24* and *BBX25*
233 expressions peak early in the day but their expression reduced around evening and
234 early night, both at 22°C and 27°C (Figure 2A). Interestingly, their expression is
235 significantly upregulated at 27°C than at 22°C both under SD (Figure 2A) and LD
236 (Supplemental Figure S5B and C) conditions. Moreover, immunoblot analysis of the
237 *35S::BBX24-GFP* line revealed that BBX24 protein levels was elevated at 27°C
238 compared to 22°C, specifically at ZT2 (Supplemental Figure S5D). Further, when we
239 monitored BBX24 protein accumulation at different ZT times, we found that at ZT0,
240 BBX24 protein was hardly detectable, and the protein stabilized in response to light
241 and reached the peak at ZT2 and then reduced at ZT4 and ZT8 at 22°C (Figure 2B).
242 However, at 27°C, BBX24 protein abundance increased nearly two-fold over 22°C
243 at ZT2, and the protein level was largely comparable between 22°C and 27°C at ZT4
244 and ZT8 (Figure 2B). Similarly, immunoblot analysis of the *35S::Myc-BBX25*
245 transgenic line revealed that at ZT2, BBX25 protein levels was also elevated at 27°C
246 compared to 22°C under SD (Supplemental Figure S5E). Specifically, BBX25 protein
247 was more stable at ZT2 and ZT4 at 27°C compared to 22°C (Figure 2C). Unlike
248 BBX24, BBX25 was detectable at the end of the night (ZT23), but its levels was not
249 altered at 27°C (Figure 2C). Consistent with the increased accumulation of BBX24
250 protein in response to 27°C, microscopic analysis of *35S:BBX24:GFP* seedlings
251 revealed that BBX24-GFP was more prominent in the hypocotyl region as relative

252 fluorescence of GFP was significantly increased at 27°C than at 22°C (Figure 2D-
253 2E), while no fluorescence was detected in Col-0 (Supplemental Figure S5F).
254 Subsequently, we also observed an increased number of cells with BBX24-GFP
255 fluorescence in seedlings grown at 27°C compared to 22°C (Figure 2F). Together,
256 these results suggest that warm temperatures promote BBX24 and BBX25 gene
257 expression and protein accumulation.

258 **BBX24/BBX25 are essential for the accumulation of PIF4 protein in response**
259 **to warm temperature**

260 As our above results indicate that BBX24/BBX25 are required for the optimal
261 expression of growth and hormone-related genes in response to warm
262 temperatures, we wanted to know if this is due to differential PIF4 protein
263 abundance. Our immunoblot data from SD-grown seedlings at 22°C revealed that at
264 the end of the night (ZT23), PIF4 protein levels was reduced in the *bbx24bbx25*
265 double mutant than Col-0, while during the day time it was more or less similar to
266 Col-0 (Figure 3A). Interestingly, at 27°C, the PIF4 protein levels was strongly
267 reduced in the *bbx24bbx25* double mutant at the end of the night (ZT23) and during
268 the day (ZT2-ZT8) compared to Col-0 (Figure 3A). However, in Col-0, PIF4 levels
269 stayed very high at the end of the night (ZT23) and throughout the day (ZT2-ZT8)
270 (Figure 3A). Supporting this, when 22°C grown seedlings under SD were treated
271 with 27°C for short durations (0, 2, 4, 8h), the PIF4 protein levels in Col-0 increased
272 with the duration of warmth treatment (Figure 3B). However, in the *bbx24bbx25*,
273 PIF4 fails to accumulate in response to warm and its levels stayed very low than Col-
274 0 (Figure 3B). Consistently, overexpression of *BBX24* and *BBX25* also resulted in
275 increase in PIF4 protein levels at 22°C and 27°C compared to Col-0 (Figure 3C).
276 BBX24/BBX25 was shown to inhibit photomorphogenesis by interfering with the HY5
277 transcriptional activity (Gangappa *et al.*, 2013). Therefore, we wanted to see if
278 BBX24/BBX25-mediated thermosensory hypocotyl growth is due to altered HY5
279 protein status. Our immunoblot data suggests that HY5 protein levels were
280 comparable between *bbx24bbx25* double mutant and Col-0 both at 22°C and 27°C
281 (Figure 3D), confirming that BBX24/BBX25-mediated thermosensory hypocotyl

growth is not due to reduced HY5 levels but due to enhanced PIF4 protein accumulation. Together, these results suggest that the BBX24/BBX25 function is crucial for promoting PIF4 protein abundance in response to warmth both during night and daytime.

Next, we wanted to see if BBX24/BBX25 also affects *PIF4* at the transcriptional level; we checked its transcript levels and found that *PIF4* expression is moderately but significantly downregulated in the *bbx24bbx25* mutant while upregulated in *BBX24* and *BBX25* overexpression transgenic lines at the end of the night (ZT23), both at 22°C and 27°C under SD (Supplemental Figure S6A). However, the regulation of *PIF4* gene expression by BBX24/BBX25 is likely indirect, as our ChIP analysis followed by qPCR data revealed that BBX24/BBX25 did not bind to the *PIF4* promoter (Supplemental Figure S6B-D). Furthermore, ChIP analysis also indicates that BBX24/BBX25 do not bind to the promoters of PIF4 targeted growth-responsive genes (Supplemental Figure S6E-G).

Further, when we treated five-day-old seedlings with proteasomal inhibitor MG132, we found that protein stability increased in the *bbx24bbx25* double mutant compared to mock-treated seedlings (Figure 3E). However, it was still visibly reduced compared to MG132-treated Col-0 seedlings (Figure 3E and 3F). Consistent with this, when we treated seedlings with a translation inhibitor, cycloheximide (CHX), we found that PIF4 degradation was significantly faster in the *bbx24bbx25* mutant, specifically at 60 and 120 min of CHX treatment, compared to Col-0 (Figure 3G and 3H). Together, these data suggest that BBX24 and BBX25 play a crucial role in *PIF4* transcript accumulation and also in maintaining its protein abundance at the posttranslational level.

BBX24/BBX25-mediated hypocotyl elongation in response to warmth is dependent on PIF4

As BBX24/BBX25 mediated warm temperature response is linked to enhanced PIF4 protein accumulation, we wanted to check the genetic interaction of BBX24/BBX25 with PIF4. We introduced *pif4* mutation into *BBX24-OE* and *BBX25-OE* lines through genetic crosses and generated homozygous lines. Analysis of hypocotyl length

312 revealed that the exaggerated hypocotyl growth of the *BBX24-OE* line was strongly
313 suppressed in the *pif4* mutant background as the hypocotyl length of *BBX24-OE pif4*
314 was close to the *pif4* mutant (Supplemental Figure S7A and B). Similarly, the *BBX25-*
315 *OE pif4* hypocotyl growth was markedly suppressed compared to the *BBX25-OE* line
316 (Supplemental Figure S7A and B). These results confirm that BBX24/BBX25-
317 mediated thermosensory hypocotyl growth strongly depends on the PIF4, implying
318 that BBX24/BBX25 probably acts upstream of PIF4.

319 **BBX24/BBX25 function is essential for PIF4-mediated thermosensory growth**

320 Consistent with the above results that BBX24/BBX25 are critical for maintaining PIF4
321 protein abundance, our genetic analysis also revealed that BBX24/BBX25 are
322 necessary for PIF4-mediated thermosensory growth (Figure 4). We have introduced
323 *bbx24*, *bbx25* and *bbx24bbx25* mutations in the *pPIF4:PIF4-FLAG* transgenic line,
324 which overexpresses PIF4 (Gangappa et al., 2017) (hereafter referred to as *PIF4-*
325 OE) (Supplemental Figure S8A) and analyzed their hypocotyl phenotypes. The
326 *bbx24* or *bbx25* single mutants showed moderate suppression, while the
327 *bbx24bbx25* strongly suppressed the exaggerated hypocotyl and cotyledon
328 phenotype of the *PIF4-OE* line at 22°C and 27°C under SD (Figure 4A-4D;
329 Supplemental Figure S8B-E). Similar to SD, under LD 22°C, *bbx24* and *bbx25*
330 mutations showed additive effects in suppressing the cotyledon phenotype of the
331 *PIF4-OE* line (Supplemental Figure S8F and G). Consistent with the growth
332 suppression, *bbx24bbx25* strongly suppressed the expression of growth-promoting
333 genes such as *YUC8*, *IAA19*, *XTR7*, *SAUR22* and *PRE5* in the *PIF4-OE* line
334 (Supplemental Figure S9A).

335 Notably, in line with the reduced growth and gene expression phenotype, the PIF4
336 protein levels was moderately reduced in the single mutants but almost undetectable
337 in the double mutant background both at the end of the night (Figure 4E) and during
338 the day (Supplemental Figure S9B). Similarly, when 22°C SD grown seedlings were
339 exposed to short-term warmth (27°C) for 24h, the PIF4 protein levels was markedly
340 reduced in both *bbx24 PIF4-OE* and *bbx25 PIF4-OE* compared to *PIF4-OE* line
341 (Figure 4F). Interestingly, the PIF4 protein was almost undetectable in the

342 *bbx24bbx25 PIF4-OE* mutant (Figure 4F). Consistent with the unstable nature of the
343 PIF4 protein in the *bbx24bbx25* double mutant, we found that the *PIF4* transcript
344 accumulation was drastically reduced in the *bbx24bbx25* double mutant than Col-0,
345 both at 22°C and 27°C (Supplemental Figure S9C). Also, in line with the reduced
346 *PIF4* mRNA accumulation in the *bbx24bbx25* double mutant observed above,
347 treating *bbx24bbx25* double mutants with MG132 only partially stabilized the PIF4
348 protein (Figure 4G) further confirms that BBX24/BBX25-mediated PIF4 protein
349 accumulation is manifested both at the transcription and posttranslational level.

350 In line with the role of BBX24/BBX25 in facilitating PIF4 protein accumulation,
351 overexpression of *BBX24* or *BBX25* in the *PIF4-OE* background resulted in further
352 enhancement in the hypocotyl length while they further suppressed the small
353 cotyledon phenotype of *PIF4-OE* in SD (Supplemental Figure S9D-G) and LD
354 (Supplemental Figure S10A-D) conditions. The *PIF4-OE BBX24-OE* and *PIF4-OE*
355 *BBX25-OE* double overexpression transgenic lines showed etiolated growth with
356 very long hypocotyl and half-opened or closed cotyledons, especially at 27°C, which
357 is a characteristic phenotype of genotypes with very high PIF4 activity (Supplemental
358 Figure S9D and E). In line with the exaggerated growth phenotypes of the double
359 overexpression transgenic lines, immunoblotting data revealed that when 22°C LD
360 grown seedlings were exposed to 27°C for 4h, PIF4 protein levels was elevated in
361 the *PIF4-OE BBX24-OE* and *PIF4-OE BBX25-OE* transgenic seedlings compared
362 to *PIF4-OE* (Supplemental Figure S10E). The *PIF4* transcript levels in these *BBX24-*
363 *OE PIF4-OE* and *BBX25-OE PIF4-OE* transgenic seedlings was significantly more
364 than the Col-0 but lower than the *PIF4-OE* line, both at 22°C and 27°C under SD
365 (Supplemental Figure S10F), which is likely due to feedback regulation to regulate
366 *PIF4* threshold levels.

367 **BBX24/BBX25 physically interact with PIF4**

368 Next, to know if BBX24/BBX25-mediated PIF4 protein stabilization at the
369 posttranslational level requires direct physical interactions, we carried out a Co-
370 immunoprecipitation (Co-IP) assay. When BBX24-GFP protein was pulled down
371 using an anti-GFP antibody, we could detect PIF4 protein in the immunoprecipitated

372 complex using a native PIF4 antibody (Figure 4H), while in Col-0 (used as a negative
373 control), we didn't detect PIF4 protein, suggesting that BBX24 physically interacts
374 with PIF4 in vivo (Figure 4H). Similarly, when we pulled down Myc-BBX25 using an
375 anti-cMyc antibody, we could detect the PIF4 protein in the immunoprecipitated
376 complex (Figure 4I) but not in Col-0, implying that BBX25 physically interacts with
377 PIF4 in vivo (Figure 4I). Consistent with Co-IP data, Bimolecular Fluorescent
378 Complementation (BiFC) assays from onion epidermal cells also revealed BBX24
379 and BBX25 physically interacts with PIF4 in planta (Figure 4J). To further confirm
380 these interactions, we also performed yeast two-hybrid (Y2H) assays by cloning
381 BBX24 and BBX25 with GAL4 DNA-binding domain (DBD) and PIF4 with Activation
382 domain (AD). Our Y2H assay revealed that BBX24/PIF4 and BBX25/PIF4 co-
383 transformed colonies were able to grow on the minimal media lacking Histidine and
384 Adenine and were also able to activate the production of α-galactosidase, which
385 converts 5-Bromo-4-chloro-3-indolyl α-D-galactopyranoside (X-α-Gal) substrate into
386 and blue colour (Figure 4K). Together, these shreds of evidence confirm that BBX24
387 and BBX25 physically interact with PIF4 in vivo.

388 **ELF3 inhibits *BBX24*/*BBX25* gene expression during dawn in a temperature-**
389 **dependent manner**

390 ELF3, ELF4 and LUX ARRHYTHMO (LUX) form the Evening Complex (EC). ELF3
391 is the key component of EC as it bridges ELF4 and LUX (Nusinow *et al.*, 2011) and
392 is a crucial negative regulator of thermosensory signaling (Box *et al.*, 2015; Jung *et*
393 *al.*, 2020; Nieto *et al.*, 2015). ELF3 strongly inhibits hypocotyl growth under optimal
394 temperatures by directly inhibiting PIF4 transcription and its transcriptional activity
395 through direct physical association and sequestration (Nieto *et al.*, 2015; Nusinow *et*
396 *al.*, 2011). Our above results show that *BBX24*/*BBX25* mRNA expression peaks at
397 the beginning of the day and is drastically reduced during the end of the day through
398 to early night. However, their expression was significantly elevated under warm
399 temperatures, even during the evening, as shown above (Figure 2A). To know if
400 ELF3 inhibits *BBX24/BBX25* gene expression in the evening, we analyzed gene
401 expression through qPCR from Ws (Wild-type) and *elf3* mutant seedlings harvested

402 at ZT6 and ZT10 grown in SD. The expression of *BBX24* and *BBX25* was
403 comparable between Ws and *elf3* mutant at ZT6 (Figure 5A and 5B). Interestingly,
404 their expression is significantly increased in *elf3* mutant at ZT10 compared to Ws,
405 both at 22°C and 27°C (Figure 5A and 5B), suggesting the plausible role of ELF3 in
406 inhibiting *BBX24/BBX25* gene expression during the evening when the EC activity
407 peaks.

408 LUX is a DNA-binding component of EC and has been shown to bind to conserved
409 cis-acting variable motifs such as *AGATTCGA*, *AGATACGC*, *ATATTCGA*,
410 *AAGATCTT* and *GGATCCGA* (Chow et al., 2012; Helfer et al., 2011; Nusinow *et al.*,
411 2011; Silva et al., 2020). We looked for potential LUX binding sites to further
412 understand if ELF3 (a component of EC) can directly bind to *BBX24* and *BBX25*
413 promoters. Interestingly, the *BBX24* and *BBX25* promoters harbour potential LUX
414 binding motifs, *GATACG* and *AAGATCG*, respectively (Figure 5C and D), which are
415 similar to the previously reported motifs bound by LUX (Silva *et al.*, 2020). We carried
416 out a Chromatin Immunoprecipitation (ChIP) assay using a *35S::ELF3-YFP*
417 transgenic line expressing stable protein at ZT10 under 22°C and 27°C under SD
418 (Supplemental Figure 11A). Our ChIP qPCR results revealed a significant
419 enrichment of ELF3 onto the *BBX24* and *BBX25* promoters at the region containing
420 the LUX-Binding site in the IP samples compared to mock (preimmune serum)
421 (Figure 5E and 5F). However, the binding of ELF3 to *BBX24* and *BBX25* promoters
422 was strongly inhibited at 27°C grown seedlings (Figure 5E and 5F). This is also
423 consistent with the earlier reports that EC binding to the target DNA was
424 compromised at warm temperatures (27°C) (Silva *et al.*, 2020). In summary, our
425 study demonstrates *BBX24*/*BBX25* as novel targets of EC for transcriptional
426 repression at lower temperatures to inhibit growth, while warm temperature-
427 mediated inhibition of ELF3 activity relieves this repression.

428 **BBX24/BBX25 genetically act downstream to ELF3**

429 Our above results suggest that BBX24/BBX25 have an impact on PIF4 at both
430 protein and transcript levels. ELF3, a potent negative regulator of PIF4, inhibits *PIF4*
431 transcription and also forms heterodimers and sequesters it (Box *et al.*, 2015; Nieto

432 *et al.*, 2015; Nusinow *et al.*, 2011). As ELF3 binds to the *BBX24*/*BBX25* promoter to
433 suppress their gene expression, we hypothesize that ELF3 could be the possible
434 target through which BBX24/BBX25 regulates PIF4 functions. To address this, we
435 performed epistatic interactions by generating *elf3bbx24*, *elf3bbx25* and
436 *elf3bbx24bbx25* mutants. Measurement of hypocotyl length of double, triple and
437 parental genotypes along with WT (segregated from Col-0xWs) suggests that while
438 *bbx24* moderately suppressed, *bbx25* showed weaker suppression of long hypocotyl
439 phenotype (Supplemental Figure S11B and C) and smaller cotyledon area of *elf3*
440 mutant (Supplemental Figure S11D and E). However, *bbx24bbx25* could strongly
441 suppress the long hypocotyl phenotype of *elf3* mutant, as *bbx24bbx25elf3* hypocotyl
442 length was significantly shorter (Figure 6A and 6B). In contrast, the cotyledon area
443 of *bbx24bbx25elf3* was significantly bigger than *elf3* mutant (Supplemental Figure
444 S11F and G), suggesting that *elf3* growth phenotypes are strongly dependent on
445 BBX24/BBX25.

446 As our genetic and molecular data reveal that BBX24/BBX25 probably function
447 downstream to ELF3 but upstream to PIF4, we wanted to see if the suppression of
448 *elf3* growth phenotype by *bbx24bbx25* is due to reduced PIF4 protein levels.
449 Interestingly, our immunoblot data from six-days-old 22°C SD-grown seedlings or
450 22°C SD-grown seedlings exposed to 27°C for 24h indeed showed that PIF4 protein
451 levels was markedly reduced in the *bbx24bbx25elf3* triple mutant compared to *elf3*
452 mutant both at 22°C and 27°C (Figure 6C). Moreover, increased PIF4 accumulation
453 in *elf3* mutant at ZT23 and ZT8 in 22°C and 27°C grown seedlings was found to be
454 dependent on BBX24/BBX25, as PIF4 protein levels was strikingly reduced in the
455 *bbx24bbx25elf3* triple mutant (Supplemental Figure 12A). The increased PIF4
456 protein levels in the *elf3* mutant is likely due to increased accumulation of *PIF4*
457 transcript. In line with this, we found that the *PIF4* transcript levels was significantly
458 reduced in the *bbx24bbx25elf3* triple mutant compared to *elf3* (Supplemental Figure
459 S12B). Consistent with the suppression of *elf3* phenotype by *bbx24bbx25*, the
460 expression of PIF4-regulated growth genes such as *XTR7*, *IAA19*, *PRE5,* and *IAA29*
461 are significantly downregulated in the *bbx24bbx25elf3* mutant background than *elf3*
462 (Supplemental Figure S12C). Together, these results confirm that BBX24/BBX25-

463 mediated inhibition of ELF3 function is necessary for optimal PIF4 gene expression
464 and protein accumulation.

465 Consistent with the role of BBX24/BBX25 in thermosensory hypocotyl and cotyledon
466 growth, we also found that they play an important role in later developmental stages,
467 such as petiole elongation and flowering. We found that long petiole and early
468 flowering phenotypes of *PIF4-OE* and *elf3* mutants were strongly suppressed by
469 *bbx24bbx25* mutations both under SD (Supplemental Figure S13) and LD
470 (Supplemental Figure S14) conditions.

471 **BBX24/BBX25 antagonizes ELF3 to facilitate PIF4 function**

472 As our above data suggest that BBX24/BBX25 functions antagonistic to ELF3, we
473 hypothesized that BBX24/BBX25 might inhibit ELF3 activity to promote PIF4
474 functions. To further test this, we introduced *BBX24-OE* and *BBX25-OE* transgenes
475 into the *ELF3-OE* background, generated *BBX24-OE ELF3-OE* and *BBX25-OE*
476 *ELF3-OE* double homozygous transgenic lines and analyzed their hypocotyl
477 phenotype. Measurement of hypocotyl length from SD-grown seedlings at 22°C and
478 27°C revealed that overexpression of *BBX24* or *BBX25* significantly suppressed the
479 short hypocotyl phenotype of the *ELF3-OE* transgenic line (Supplemental Figure
480 S15A and B). Consistent with this, our immunoblot data using ELF3 specific antibody
481 (Supplemental Figure S15D) revealed that ELF3 protein level is elevated in the
482 *bbx24bbx25* double mutant but markedly reduced in the *BBX24* and *BBX25*
483 overexpression lines compared to Col-0 (Figure 6D). In contrast to the effect of
484 *bbx24bbx25* mutations in increasing ELF3 protein levels, *ELF3* gene expression was
485 not altered in the *bbx24bbx25* double mutant compared to Col-0 (Supplemental
486 Figure 15C). Further, consistent with the suppression of short hypocotyl length of
487 *ELF3-OE* line by *BBX24-OE* and *BBX25-OE*, we found that, overexpression of
488 *BBX24* and *BBX25* strongly recovered the reduced PIF4 protein levels of *ELF3-OE*
489 line (Figure 6E) indicating negative inhibitory effects of BBX24/BBX25 on ELF3 to
490 facilitate PIF4 protein accumulation.

491 Next, to know if BBX24/BBX25-mediated inhibition of ELF3 function requires direct
492 physical interactions, we carried out a Co-IP assay. We used *35S:BBX24-GFP*

493 transgenic lines and pulled down BBX24-GFP from the total protein extract using an
494 anti-GFP antibody. In the BBX24-GFP immunoprecipitated complex, we could detect
495 ELF3 as revealed by immunoblotting using a native anti-ELF3 antibody, but not in
496 the Col-0 (Figure 6F). Similarly, when we pulled down from the total protein extract
497 of *35S:Myc-BBX25* transgenic line, we could detect ELF3 in the immunoprecipitated
498 complex but not in Col-0 (Figure 6G), indicating that BBX24 and BBX25 physically
499 interact with ELF3 in vivo. To support these physical interactions, we performed a
500 BiFC assay and found that BBX24 and BBX25 physically interact with ELF3 in planta
501 in onion epidermal cells (Figure 6H, Supplemental Figure S15E). When we co-
502 transformed BBX24-nYFP/ELF3-cYFP and BBX25-nYFP/ELF3-cYFP constructs,
503 we observed reconstitution of uniform YFP fluorescence in the nucleus (Figure 6H).
504 Interestingly, we also observed two or more discrete condensates in the nucleus
505 (Figure 6H; Supplemental Figure 15F). Furthermore, Y2H assays, using ELF3 as
506 bait and BBX24 and BBX25 as prey, found that BBX24 and BBX25 physically
507 interact with ELF3 (Figure 6I). The BD-BBX24/AD-ELF3 and BD-BBX25/AD-ELF3
508 combinations of constructs, when transformed onto Y2H-Gold reporter strain, they
509 grew on the synthetic minimal media lacking Histidine and Adenine and also, these
510 colonies developed blue colour in the presence of X-α-Gal substrate (Figure 6I).
511 Together, our genetic and biochemical data confirm that BBX24/BBX25 inhibit ELF3
512 function to promote PIF4-mediated thermomorphogenic growth.

513 DISCUSSION

514 Rising global temperatures due to climate change profoundly affect plant health and
515 pose a significant threat to crop yields (Burroughs *et al.*, 2023; Koester *et al.*, 2014;
516 Peng *et al.*, 2004; Zhao *et al.*, 2017). While plants have evolved intricate signaling
517 mechanisms to sense, integrate, and adapt to temperature fluctuations, the
518 underlying signaling mechanisms are poorly understood. As PIF4 is the central
519 component of thermomorphogenesis, maintaining its protein abundance is crucial in
520 achieving optimal thermomorphogenic growth both during the night and daytime.
521 BBX proteins have emerged as crucial signaling nodes for orchestrating adaptive
522 responses to diverse environmental signals such as light, shade, and abiotic

523 stresses (Ding *et al.*, 2018; Gangappa and Botto, 2014; Podolec et al., 2022; Song
524 *et al.*, 2020; Tripathi et al., 2017; Vaishak *et al.*, 2019; Wang et al., 2014; Zhao et al.,
525 2020). This study discovers that BBX24/BBX25 are novel and essential components
526 of the thermosensory signaling pathway and act to promote PIF4 function by
527 inhibiting its critical repressor, ELF3 (Figure 7).

528 Our study demonstrates that BBX24/BBX25 play a positive regulatory role in
529 temperature-responsive hypocotyl growth (Figure 1). BBX24/BBX25 functions
530 exhibit significant overlap, as evidenced by a more pronounced reduction in cell
531 length and hypocotyl growth in the *bbx24bbx25* double mutant than in the *bbx24* and
532 *bbx25* single mutants at warm temperature, as opposed to *BBX24-OE* and *BBX25-*
533 *OE* overexpression lines that promoted cell elongation and hypocotyl growth (Figure
534 1). Consistent with the growth phenotypes, *bbx24bbx25* double mutants had
535 reduced expression of PIF4 target genes such as *XTR7*, *YUC8*, *EXP8*, *IAA19*, etc.,
536 involved in hormone biosynthesis and signaling both at night and during the day
537 (Figure 1; Supplemental Figure S4), which is in line with the reduced PIF4 protein
538 accumulation in response to warm temperatures (Figure 3). Contrary to *bbx24bbx25*
539 mutants, the enhanced thermomorphogenic response and gene expression of the
540 *BBX24-OE* and *BBX25-OE* lines, was consistent with the increased PIF4 protein
541 levels (Figure 3C). Our genetic analysis demonstrates that BBX24/BBX25-mediated
542 thermomorphogenic response is directed through PIF4 (Supplemental Figure S7).
543 In agreement with the BBX24/BBX25 acting through PIF4, the genetic analysis also
544 revealed that the absence of *BBX24* and *BBX25* strongly suppress the robust growth
545 and gene expression phenotypes of the transgenic line overexpressing *PIF4-FLAG*,
546 which is due to the reduced PIF4-FLAG protein accumulation in the single mutants,
547 while complete absence of PIF4-FLAG protein in the *bbx24bbx25* background
548 (Figure 4). The lack of PIF4-FLAG protein was somewhat surprising compared to
549 native PIF4 protein. The possible reason could be the enhanced degradation of
550 PIF4-FLAG protein over native PIF4 protein.

551 Several thermosensory signaling components such as HMR (HEMERA), RCB
552 (REGULATOR OF CHLOROPLAST BIOGENESIS), and HSFA1s (HEAT SHOCK
553 TRANSCRIPTION FACTOR 1) have been shown to stabilize PIF4 and promote

554 daytime mediated thermomorphogenic growth (Qiu *et al.*, 2021; Tan et al., 2023b).
555 Meanwhile, COP1/DET1/SPA, upstream regulators of PIF4, promote PIF4 protein
556 accumulation during the night (Gangappa and Kumar, 2017). Our study reveals that
557 BBX24/BBX25 serve as novel upstream regulators, essential for maintaining optimal
558 PIF4 levels at night and also during the day to promote thermomorphogenesis
559 (Figure 1 and 3). As BBX24/BBX25 and COP1/DET1 promote PIF4 accumulation,
560 their possible functional connection in maintaining optimal PIF4 protein levels in the
561 dark period needs further investigation. While BBX24/BBX25 largely contribute to
562 PIF4 protein accumulation by enhancing *PIF4* gene expression, likely, they are also
563 protecting PIF4 protein from its negative regulators at the post posttranslational level,
564 as revealed from our MG132 and CHX treatment experiments (Figure 3E-3H). The
565 physical interactions between BBX24/BBX25 and PIF4 (Figure 4) also provide
566 evidence that these proteins likely play a crucial role in safeguarding PIF4 from its
567 repressors.

568 Previous studies have shown that ELF3 acts upstream of PIF4 and inhibits its
569 function both at the transcription and at the protein level (Box *et al.*, 2015; Nieto *et*
570 *al.*, 2015; Nusinow *et al.*, 2011). Interestingly, our data demonstrate that the *elf3*
571 mutant growth phenotypes, gene expression, and PIF4 protein accumulation
572 strongly depend on BBX24/BBX25, suggesting that BBX24/BBX25 likely act
573 downstream to ELF3 but upstream to PIF4 (Figure 6). Our RT-qPCR and ChIP data
574 further support that ELF3 inhibits *BBX24* and *BBX25* gene expression during the
575 evening at 22°C, which is nullified at 27°C (Figure 5), due to warm temperature-
576 mediated inactivation of ELF3 activity (Jung *et al.*, 2020). Nevertheless, our
577 immunoblot data revealed that BBX24/BBX25 inhibit ELF3 protein accumulation at
578 warm temperatures (Figure 6D). Therefore, in addition to warm temperature-
579 mediated inhibition of ELF3 activity through liquid-liquid phase separation (LLPS),
580 BBX24/BBX25 inhibit ELF3 function by reducing ELF3 accumulation. Moreover, the
581 physical association of BBX24/BBX25 could also sequester with ELF3, resulting in
582 enhanced PIF4 function (Figure 6). This is also supported by genetic data, wherein
583 *BBX24-OE* and *BBX25-OE* significantly suppressed the short hypocotyl phenotype
584 and reduced PIF4 accumulation in the *ELF3-OE* transgenic line (Figure 6E;

585 Supplemental Figure S15A and B). Therefore, we propose that constitutive
586 thermomorphogenic response and high PIF4 activity in the *elf3* mutant is not solely
587 attributed to the alleviation of transcriptional repression on PIF4 but also due to the
588 concurrent increase in BBX24/BBX25 activity, and these dual mechanisms together
589 potentiate thermomorphogenic response (Figure 6; Supplemental Figure S11 and
590 S12).

591 Consistent with the role of BBX24/BBX25 in promoting PIF4 function, the PIF4-
592 mediated thermosensory petiole growth and flowering are also dependent on PIF4
593 both under SD and LD photoperiods, highlighting their role beyond seedling
594 development (Supplemental Figure S13 and S14). These pieces of evidence reveal
595 that BBX24/BBX25 proteins act as key regulators of growth and development in
596 response to varying light and temperature cues by coordinating clock and external
597 cues. In summary, we propose the ELF3-BBX24/BBX25-PIF4 as a novel regulatory
598 module (Figure 7), critical for integrating temperature and light cues to regulate
599 thermosensory growth and development in Arabidopsis.

600 **METHODS**

601 **Plant Material and Growth Conditions**

602 All the lines used here are in Columbia-0 (Col-0) background except *elf3*-4, which is
603 in Wassilewskija (WS) background. The genotypes *bbx24-1* (Gangappa *et al.*, 2013),
604 *bbx25-2* (Gangappa *et al.*, 2013) *35S::BBX24-GFP*(Job *et al.*, 2018), *pPIF4*::*PIF4-*
605 *FLAG* (Gangappa *et al.*, 2017), *pif4-101* (Lorrain *et al.*, 2008), and elf3-4 {Dixon,
606 2011 #2021), have been described previously. For hypocotyl experiments, seeds
607 were surface sterilized with 70% ethanol containing 0.5% Triton X-100 for 10 minutes
608 and plated on half-strength Murashige and Skoog (MS) medium (Sigma-Aldrich)
609 supplemented with 1% sucrose, 0.5 mM MES (pH-5.7) and 0.8% agar following
610 stratification at 4°C for four-days. For the hormone experiments, seeds were plated
611 on MS media containing different concentrations of hormones or their inhibitors.
612 Upon seed germination at 22°C long day (16h Light/8h Dark) growth chamber
613 (Percival Scientific) seedlings were transferred to respective 22°C and 27°C short

614 day (8h Light/16h Dark) conditions or as stated in the experimental conditions with
615 70% humidity and light intensity of 100 µmol m^{-2} sec^{-1}. Five days after germination
616 (six-day-old), seedlings were taken for the hypocotyl length and cotyledon area
617 measurements using ImageJ software. At least 25 seedlings for each genotype were
618 taken for the measurements.

619 **Generation of *BBX25* overexpression transgenic lines**

620 For the generation of *35S::Myc-BBX25* overexpressing transgenic lines, the full-
621 length BBX25 coding sequence was amplified from 22°C LD grown Col-0 cDNA and
622 cloned into the pENTR vector through pENTR™ Directional TOPO® Cloning Kits
623 (Invitrogen), which is then subcloned into the destination vector pGWB618
624 (Nakamura et al., 2010) using LR cloning kit (Invitrogen). The binary expression
625 cassette is then transformed into *Agrobacterium tumefaciens* GV3101 strain.
626 Agrobacterium harbouring the transgene were transfected into Col-0 through the
627 floral dip method. Positive transformants were selected on ½ MS containing 7.5
628 ug/ml glufosinate-ammonium (BASTA). Four independent lines showing 3:1
629 segregation on BASTA were chosen for further analysis. In the T_3 generation, these
630 lines were selected based on transgene and protein expression analysis for further
631 analysis.

632 **Generation of double and triple mutants**

633 For the generation of double mutants *bbx24-1bbx25-2*, *bbx24-1 PIF4-*
634 *OE*, *bbx25-2 PIF4-OE*, *BBX24OE pif4-101*, *BBX25-OE pif4-101*, *bbx24-1 elf3-4*,
635 *bbx25-2 elf3-4*, *BBX24-OE PIF4-OE*, *BBX25-OE PIF4-OE*, *BBX24-OE ELF3-OE*
636 and *BBX25-OE ELF3-OE* we crossed *bbx24-1* and *bbx25-2* with each other and
637 *bbx24-1*, *bbx25-2*, *BBX24-OE* and *BBX25-OE* with the respective genotypes. For
638 the generation of triple mutants *bbx24-1 bbx25-2 PIF4-OE* and *bbx24-1 bbx25-2*
639 *elf3-4* we crossed homozygous double mutant of *bbx24-1 PIF4-FLAG* with *bbx25-2*
640 *PIF4-FLAG* and *bbx24-1elf3-4* with *bbx25-2elf3-4*, respectively. After crossing, we
641 got F_1 seeds that grew for one more generation to get F_2 seeds. Approximately 20-
642 30 F_2 seedlings growing on antibiotic selection were picked up where homozygosity
643 was confirmed through PCR-based genotyping method using gene-specific and T-

644 DNA specific primers. T-DNA-specific primers used were SALK LB1.3 for *bbx24-1*,
645 SAIL LB3 for *pif4-101*, and *spm1* for *bbx25-2*. For *elf3-4* genotyping, we amplified
646 PCR fragments using dCAPS primers followed by AluI restriction digestion. To
647 confirm the homozygosity of *BBX24-OE*, *BBX25-OE*, *PIF4-FLAG* and *ELF3-OE*, we
648 first confirmed the presence of CDS using PCR, followed by the survival of seedlings
649 on an antibiotic selection plate in the next generation. F_3 generation seedlings
650 showing 100% survival on double antibiotic selection were used for further
651 experiments. Primers used for genotyping are listed in Table S1.

652 **Gene expression analysis**

653 Approximately 100 mg seedlings from the indicated genotypes and growth
654 conditions were harvested, frozen in liquid nitrogen, and stored at -80°C until further
655 processing. For RNA extraction, seedlings were ground to a fine powder in liquid
656 nitrogen, and total RNA was isolated using an RNeasy plant mini kit (Qiagen)
657 following the kit protocol with on-column DNase I digestion (Qiagen) for 30 min. at
658 RT. 1.5 µg of total RNA was converted into cDNA using SuperScript® III First-Strand
659 Synthesis kit (Invitrogen) by taking Oligo$(dT)_{20}$ primers following manufacturer's
660 instructions. For RT-qPCR, nuclease-free water-diluted cDNA was mixed with
661 PowerUp™ SYBR™ Green Master Mix (ThermoFisher Scientific) and gene-specific
662 primers. Each gene RT-qPCR reaction was set in triplicate with a Biorad CFX96
663 Touch Real-Time PCR Detection System or an Applied Biosystems™ 7500 Fast
664 Real-Time PCR System. The transcript level of each gene was calculated relative to
665 that of EF1α. RT-qPCR results were analyzed in fold change using the $2^{-\Delta\Delta Ct}$ method.

666 **Protein extraction and Immunoblotting**

667 For western blotting, approximately 100-150 mg tissue of six-day-old *Arabidopsis*
668 seedlings grown in different experimental conditions were harvested in a
669 microcentrifuge tube, snap-frozen and ground to fine powder in liquid nitrogen. Total
670 protein was extracted in 250 µl of protein extraction buffer containing 50 mM Tris-
671 HCl pH 8.0, 150 mM NaCl, 10% glycerol, 5mM DTT, 1% NP-40, 0.5mM PMSF, and
672 1X EDTA free Protease Inhibitor Cocktail (Roche).
673 After resuspending in the extraction buffer, crude protein samples were cleared by

674 centrifuging at 15,000 rpm for 10 min at 4°C. Protein concentration was estimated
675 using Bradford reagent (Biorad). Approximately 30 µg of total protein was boiled at
676 95°C for 5 minutes in 5x SDS gel loading dye (100 mM Tris-HCL pH 7.5, 12%
677 glycerol, 4% SDS, 200 mM DTT, 40 mM β-ME and 0.001% bromophenol blue),
678 separated via SDS-PAGE and transferred to the PVDF membrane (Millipore, Sigma)
679 by wet transfer method.

680 For protein detection, blots were blocked with 5% skim milk in TBST for 2h at RT,
681 incubated overnight at 4°C with respective primary antibodies, followed by
682 incubation in 1:10,000 dilutions of horseradish peroxidase-conjugated rabbit anti-
683 goat (Thermo Fisher Scientific, 811620) or goat anti-rabbit (Abcam, ab205718)
684 secondary antibodies at room temperature for 1 h. Primary antibodies used were
685 polyclonal goat anti-PIF4 antibodies (Agrisera, AS16 3955, 1:2500), polyclonal rabbit
686 anti-GFP antibodies 1:7500 (Abcam, ab290), monoclonal rabbit anti-GFP (Invitrogen
687 G10362, 1:500) monoclonal HRP conjugated mouse anti-myc (HRP) antibodies
688 (Abcam, ab62928, 1:5000), monoclonal HRP conjugated mouse anti-FLAG
689 antibodies (Abcam, ab49763, 1:5000), polyclonal rabbit anti-HY5 antibodies
690 (Agrisera, AS12 1867, 1:2500), polyclonal rabbit anti-ELF3 antibodies (Agrisera,
691 AS18 4168, 1:2000) polyclonal rabbit anti-actin antibodies (Abcam, ab197345,
692 1:10,000), and Rabbit polyclonal anti-Histone H3 antibodies, 1:10,000 (abcam,
693 ab1791). The chemiluminescence signal was detected using the SuperSignal West
694 Femto kit (Thermo Fisher Scientific) and Syngene gel-doc system. Protein band
695 intensities were measured using the ImageJ software (https://imagej.nih.gov/).

696 **MG132 and CHX treatment**

697 Mg132 and CHX treatments were carried out as reported (Zhou et al., 2021) with
698 minor modifications. For MG132 treatment, five-day-old *Arabidopsis* seedlings were
699 transferred to liquid MS medium containing 50µM MG132 or DMSO and then
700 incubated for 8 h or 16 h before tissues were harvested for immunoblot. To
701 determine the degradation rate of PIF4 protein by blocking de novo protein
702 synthesis, five-day-old 22°C SD grown seedlings treated with MG132 as above
703 before shifting to 27°C for 8hrs were washed five times and then transferred to liquid

704 MS medium supplemented with 200μM CHX followed by tissue harvest at different
705 time points for western blot analysis.

706

707 **Chromatin Immunoprecipitation (ChIP) assay**

708 ChIP assays were performed as previously described (Yamaguchi et al., 2014) with
709 modifications. Approximately 1.5 g of *35S::ELF3-YFP*(*elf3-4*) seedlings grown for
710 five days after germination at 22°C SD and 27°C SD were harvested and cross-
711 linked with 30 ml of 1% formaldehyde in 1X PBS for 2 x 10 mins by vacuum
712 infiltration. Crosslinking was quenched by adding 125 mM glycine under vacuum for
713 another 5 min. Fixed seedlings were rinsed with 30 ml 1X PBS twice, dried on stacks
714 of filter paper, frozen in liquid nitrogen and stored at -80°C. Frozen samples were
715 crushed in liquid N_2 until they became light green and homogenized in 30 ml of
716 extraction buffer I (10 Tris-HCL pH 8, 0.4M sucrose, 10 mM MgCl2, 5mM β-
717 Mercaptoethanol, 2 mM PMSF and 1X protease inhibitor cocktail). Lysate was
718 passed through 2 layers of Miracloth to remove debris and centrifuged at 1000 x g
719 for 20 minutes at 4°C to pellet down cell organelles. Pellet resuspended in 5ml of
720 extraction buffer II (10 mM Tris-HCL pH 8, 0.25M sucrose, 10 mM MgCl2, 1% Triton
721 X-100, 5mM β-Mercaptoethanol, 2 mM PMSF and 1X protease inhibitor cocktail) to
722 burst other cell organelles and centrifuged at 1000 x g for 10mins at 4°C. The
723 deposited pellet was then dissolved in 300 μl of extraction buffer III (10 mM Tris-HCL
724 pH 8, 1.7 M sucrose, 2mM MgCl2, 0.15% Triton X-100, 5mM β-Mercaptoethanol,
725 2mM PMSF and 1X protease inhibitor cocktail) which was carefully layered at the
726 top of 600 μl extraction buffer III and centrifuged at 16,000 x g for 1hr at 4°C to
727 concentrate nuclei. The nuclear pellet was dissolved in 300 μl of sonication buffer,
728 and chromatin was sheared by sonicating for 20 cycles for 30 sec. ON/OFF.
729 Sonicated samples were cleared by centrifuging at 12000 x g for 10 mins. 1/10th of
730 the sonicated sample was kept at -20°C as input, and the rest was diluted 10-fold in
731 ChIP dilution buffer for immunoprecipitation. Protein-DNA complexes were
732 immunoprecipitated by incubating the diluted chromatin overnight at 4°C with 15 μl
733 of Dynabeads Protein-G (Invitrogen) equilibrated with 2 μg of anti-GFP antibody

734 (Takara Bio, 632381). Beads were washed for 2 x 10 mins in low salt wash buffer, 1
735 x 10 mins in high salt wash buffer, 1 x 10 min in LiCl wash buffer, and 2 x 10 min in
736 TE buffer. DNA from input and IP were eluted by incubation with 10% chelex 100-
737 resin (Biorad) at 95°C for 10mins followed by 20 µg of Proteinase K treatment at
738 37°C for 30 min. The supernatant was collected after centrifuging at 16000 x g for 2
739 min., followed by the precipitation of DNA through the phenol-chloroform extraction
740 method. Precipitated DNA was dissolved in 50 µl of nuclease-free water, and 2 µl
741 was used per reaction for chip-qPCR.

742 For the ChIP assay of BBX24/BBX25 binding on *PIF4* and its target genes promoter,
743 we have used six-day-old *35S:BBX24-GFP* and *35S:Myc-BBX25* seedlings grown
744 at 27°C and tissues were harvested at ZT2 and ZT4, respectively. Further, we have
745 processed the tissues in a similar way as described above for ELF3 ChIP analysis.
746 Primers used for ChIP-qPCR analysis are listed in Supplemental Table 1.

747 **Yeast two-hybrid (Y2H) assay**

748 Y2H assay was performed following the Matchmaker® Gold Yeast Two-Hybrid
749 System User Manual (Takara Bio). Briefly, full-length coding sequences of *BBX24*
750 and *BBX25* were cloned into the bait vector pGBKT7 containing DNA-Binding
751 Domain (DBD), while PIF4 and ELF3 were cloned into the prey vector pGADT7
752 having Activation Domain (AD). For checking the protein-protein interactions,
753 different combinations of bait and prey constructs were co-transformed into Y2H
754 Gold yeast strain (Clontech) using Yeastmaker™ Yeast Transformation kit
755 (Clontech), and transformants were selected on double dropout medium SD/-Leu/-
756 Trp at 30°C for three-days. For confirmation of protein-protein interactions, overnight
757 grown double dropout screened yeast cells were diluted to an OD_{600} of 0.5 with 4X
758 serial dilutions were spotted on quadruple dropout medium SD/-Leu/-Trp/-Ade/-His
759 supplemented with X-alpha-gal. Plates were grown at 30°C for 72 hr before taking
760 the picture.

761 **Co-Immunoprecipitation**

762 Coimmunoprecipitation assays were performed using Dynabeads™ Protein G
763 Immunoprecipitation Kit (Invitrogen). Approximately 500 mg of six-day-old seedlings
764 grown at 27°C for BBX24/BBX25-PIF4 and at 22°C for BBX24/BBX25-ELF3
765 immunoprecipitation, harvested at ZT2 and ZT8 were used, respectively. Harvested
766 seedlings were grounded in liquid nitrogen, and the powder was homogenized in 1
767 ml of co-immunoprecipitation buffer containing 50 mM Tris-HCL pH-8, 100 mM NaCl,
768 10% glycerol, 2mM DTT, 1mM EDTA, 0.1% NP-40, 1mM PMSF, and 1X protease
769 inhibitor cocktail. Crude protein extract was cleared by two rounds of centrifugation
770 at 13000 rpm for 10 mins at 4°C. An aliquot of 100 µl was boiled in 5X SDS loading
771 dye as an input. The remaining 900 µl protein lysate was incubated with 50 µl
772 Dynabeads (Invitrogen) equilibrated with anti-GFP or anti-cMyc antibody at 4°C for
773 6 h. Then, beads were washed, and immunoprecipitated proteins were eluted by
774 boiling the beads at 70°C for 10 minutes in 1X Laemmli buffer. Then, input and
775 immunoprecipitated protein samples were subjected to SDS-PAGE for
776 immunodetection. For immunoprecipitation assay of BBX24-GFP/Myc-BBX25-PIF4
777 polyclonal rabbit anti-GFP (Abcam, ab290, 1:5000), monoclonal mouse anti-myc
778 (Abcam, ab62928, 1:5000) and polyclonal goat anti-PIF4 antibodies (Agrisera
779 AS163955, 1:2500) were used. For BBX24-GFP/Myc-BBX25-ELF3
780 immunoprecipitation, monoclonal rabbit anti-GFP (Invitrogen G10362, 1:500),
781 monoclonal mouse anti-myc (Abcam, ab62928, 1:5000) and polyclonal rabbit anti-
782 ELF3 antibodies (Agrisera, AS18 4168, 1:2000) were used.

783 **Differential Interference Contrast (DIC) Microscopy for cell length**
784 **measurement**

785 For histological analysis, 6-day-old whole seedlings were fixed and cleared using
786 serial dilution of ethanol (15%, 50%, 70%, 96% and 100%), each for 15 min in a 24-
787 well plate. The seedlings were then kept in a cold room at 4˚ C overnight. On a
788 subsequent day, seedlings were rehydrated in an ethanol gradient (100%, 96%,
789 70%, 50% and 15%), each step for 15 min., after which those were washed with 0.2
790 M sodium phosphate buffer (pH=7). Aniline blue (Sigma-Aldrich, Germany) staining
791 solution was prepared as 0.1% w/v stock solution in 0.2 M sodium phosphate buffer.

792 Seedlings were stained with a 1:20 dilution of aniline blue stock solution with 0.2M
793 sodium phosphate buffer. Samples were incubated overnight at room temperature.
794 Seedlings were mounted onto chloral hydrate solution (chloral hydrate: glycerol:
795 Milli-Q water:: 8:1:2), and hypocotyls were observed using an Olympus IX81 inverted
796 microscope under differential interference contrast optics. Images were acquired
797 with cellSens Standard Software (Olympus).

798 Micrographs of six seedlings were obtained for each genotype, and their cell length
799 was considered under two different temperature conditions, 22°C and 27°C short-
800 day conditions. The cell length of hypocotyls was defined as the average number of
801 cortical cells crossing the central region of hypocotyls- the number of cells varies
802 with the genotype and the growth condition. Only the cells extending in the non-
803 dividing files were counted.

804 **Bimolecular Fluorescent Complementation (BiFC) assay**

805 For the BiFC assays, the *CDS* of *BBX24*, *BBX25*, *PIF4* and *ELF3* in the pENTR-
806 D/TOPO vectors have been recombined into pSPYNE-nYFP and pSPYCE-cYFP
807 vectors using LR-Clonase (Invitrogen) to obtain the fusion proteins. *BBX24* and
808 *BBX25* were cloned into the pSPYNE vector, whereas *PIF4* and *ELF3* were cloned
809 in the pSPYCE vector. Sequence-verified constructs were then mobilized into
810 *Agrobacterium tumefaciens* (strain GV3101) with the help of the freeze-thaw
811 method. *Agrobacterium*-mediated *in planta* transient transformation onto onion bulb
812 as reported(Xu et al., 2014) The p19 protein of the tomato bushy stunt virus has
813 been used to subdue gene silencing. For infiltration, nYFP-BBX24/c-YFP-PIF4,
814 nYFP-BBX25/cYFP-PIF4, nYFP-BBX24/c-YFP-ELF3 and nYFP-BBX25/cYFP-ELF3
815 along with the p19 combination, were used with a final concentration of OD_{600} 0.6:
816 0.6: 1.0. After infiltration, onion bulbs were kept at 28±1 °C in the dark for 72 h. The
817 infected adaxial epidermis of the bulb scale was peeled and visualized with an SP8
818 confocal microscope (Leica, Germany) using 40x objective (ex: 488 nm for YFP, ex:
819 405 nm for DAPI) and deconvoluted using Leica Lightning software. Nuclei were
820 counterstained with DAPI (1 µg/ml). A combination of nYFP-BBX24/cYFP, nYFP-
821 BBX25/cYFP, nYFP/cYFP, nYFP/cYFP-PIF4 and nYFP/cYFP-ELF3 were used as

822 the negative controls. For the BBX24/BBX25-ELF3 BiFC assay, an Olympus IX81
823 epifluorescence microscope was used, and images were acquired using ImageJ Fiji
824 software.

825

826 **Quantification of GFP fluorescence using epifluorescence microscope**

827 GFP fluorescence of BBX24-GFP was captured using an Olympus IX81 inverted
828 microscope equipped with an LED lamp. Approximately ten seedlings were taken for
829 imaging after five days of growth in the respective conditions. The BBX24-GFP
830 fusion protein was excited with a 488 nm light, and the emitted fluorescence signal
831 was detected between 500nm and 561nm range. Images were acquired, and
832 fluorescence intensity was quantified using ImageJ's Fiji software. The mean
833 fluorescence intensity was calculated by marking the area with a freehand selection
834 tool. Subsequently, relative fluorescence intensity was calculated against 27°C
835 seedlings.

836 **GUS Histochemical staining**

837 For GUS-staining six-day-old 22°C and 27°C SD grown F1 seedlings of *DR5:GUS,*
838 *BBX24-OEDR5:GUS* and *BBX25-OEDR5:GUS* seedlings were harvested at ZT2
839 and fixed in 50mM Sodium phosphate buffer containing 2% formaldehyde and 0.05%
840 Triton X-100. After fixation, the seedlings were appropriately cleaned by washing
841 them three times with 50 mM phosphate buffer. To detect the GUS activity, seedlings
842 were submerged and vacuum infiltrated for 4mins in 0.5 mg/ml 5-bromo-4chloro-3-
843 indoyl glucuronide (X-Gluc) solution containing 50mM sodium phosphate buffer,
844 5mm Na2-EDTA, 1mM potassium ferrocyanide and 1mM potassium ferricyanide
845 following incubation at 37°C for overnight. The next day, seedlings were destained
846 with 75% and 95% ethanol for 3 hours each at 37°C and observed under a
847 stereomicroscope.

848 **Quantification and statistical analysis**

849 Hypocotyl length, cotyledon area, and protein band intensities were quantified using
850 ImageJ software (https://imagej.nih.gov/). The statistically significant difference in

851 the data sets was analyzed using GraphPad Prism version 8.0
852 (https://www.graphpad.com/). One-way ANOVA or Two-way ANOVA Tukey test
853 was used for multiple groups of observations. Students' t-test was used to determine
854 the significance of two groups of observations. Details of the statistical analysis can
855 be found in the figure legends.

856 **FUNDING**

857 This study was supported by grants from the Department of Biotechnology
858 (Ramalingaswami Fellowship grant, BT/RLF/Re-entry/ 28/2017), Science and
859 Engineering Research Board (Start-up Research Grant, SRG/2019/000446),
860 Intramural grant (IISER Kolkata), Ministry of Education (MoE/STARS-1/416)
861 Government of India.

862 **ACKNOWLEDGEMENTS**

863 We thank Dr. Vinod Kumar, Prof. Salome Prat and Prof. Javier F. Botto, respectively,
864 for the *pPIF4:PIF4-FLAG*, *35S::ELF3-YFP*(*elf3-4*) and *35S::BBX24-GFP* transgenic
865 lines seeds. We thank all the members of Gangappa lab for fruitful discussions.
866 B.C.M., S.S. and V.G. acknowledge the Council of Scientific and Industrial
867 Research, Department of Biotechnology, and University Grants Commission,
868 respectively, for their doctoral fellowships. G.U acknowledges the Postdoctoral
869 Fellowship from IISER Kolkata (PDF/DBS/2021/025) and Science & Engineering
870 Research Board (SERB-PDF/2022/000529). R.C. acknowledges the KVPY
871 Fellowship from the Department of Science and Technology, Govt. of India.

872 **AUTHOR CONTRIBUTIONS**

873 S.N.G. conceptualized, designed and supervised the study, analyzed data, and
874 wrote the first and subsequent drafts of the manuscript with inputs from all the
875 authors. B.C.M. designed the study, planned and conducted most experiments,
876 collected results, analyzed the data, and helped write the manuscript draft. S.S.
877 generated *elf3* and *DR5:GUS*-related genetic lines, conducted phenotypic analysis,
878 and measured cell length. V.G. assisted in raising *pif4-101*-related genetic lines with
879 phenotypic analysis. R.C. contributed to generating novel genetic materials and

880 conducted experiments. G.U. carried out BiFC experiments. All the authors have
881 read and approved the final version of the manuscript.

882 **DATA AVAILABILITY**

883 The data presented in this study is available in the main figures and the
884 supplementary material.

885 **SUPPLEMENTAL INFORMATION**

886 **Supplemental Figure S1.** Molecular and phenotypic analysis of BBX25
887 overexpression transgenic lines.

888 **Supplemental Figure S2.** BBX24/BBX25 mediated thermosensory hypocotyl
889 growth is linked to growth-promoting hormones.

890 **Supplemental Figure S3.** BBX24/BBX25 overexpression lines show differential
891 sensitivity to Auxin and BR inhibitors.

892 **Supplemental Figure S4.** BBX24/BBX25 regulates the expression of hormone and
893 growth-related genes during the daytime.

894 **Supplemental Figure S5.** Warm temperatures promote BBX24/BBX25 transcript
895 and protein accumulation.

896 **Supplemental Figure S6.** ChIP analysis for BBX24/BBX25 enrichment on *PIF4* and
897 its target genes promoter.

898 **Supplemental Figure S7.** BBX24/BBX25 mediated thermosensory hypocotyl
899 growth depends on PIF4.

900 **Supplemental Figure S8.** BBX24/BBX25 are essential for PIF4-mediated regulation
901 of hypocotyl and cotyledon growth in response to warm temperatures.

902 **Supplemental Figure S9.** BBX24/BBX25 functions are required for PIF4-governed
903 hypocotyl and cotyledon growth at higher temperatures.

904 **Supplemental Figure S10.** Regulation of hypocotyl and cotyledon growth by PIF4
905 requires BBX24/BBX25 under LD photoperiod.

906 **Supplemental Figure S11.** ELF3 genetically interacts with BBX24 and BBX25 to
907 control thermosensory hypocotyl and cotyledon growth**.**

908 **Supplemental Fi. S12.** BBX24/BBX25 inhibit ELF3 function to promote PIF4-
909 governed thermosensory growth.

910 **Supplemental Figure S13.** ELF3-BBX24/BBX25-PIF4 module controls the
911 thermosensory flowering and petiole growth under SD photoperiod.

912 **Supplemental Figure S14.** BBX24/BBX25 is required to manifest petiole growth
913 and flowering of the *PIF4-OE* transgenic line and *elf3* mutants under LD photoperiod.

914 **Supplemental Fig S15.** BBX24/BBX25 antagonize ELF3 function.

915 **Supplemental Table S1.** List of oligonucleotides used in this study.

916
917 ## REFERENCES
918

919 **Box, M.S., Huang, B.E., Domijan, M., Jaeger, K.E., Khattak, A.K., Yoo, S.J.,**
920 **Sedivy, E.L., Jones, D.M., Hearn, T.J., Webb, A.A.R., et al.** (2015). ELF3 controls
921 thermoresponsive growth in Arabidopsis. Curr Biol **25**:194-199.
922 10.1016/j.cub.2014.10.076.

923 **Burko, Y., Willige, B.C., Seluzicki, A., Novák, O., Ljung, K., and Chory, J.** (2022).
924 PIF7 is a master regulator of thermomorphogenesis in shade. Nat Commun **13**:4942.
925 10.1038/s41467-022-32585-6.

926 **Burroughs, C.H., Montes, C.M., Moller, C.A., Mitchell, N.G., Michael, A.M., Peng,**
927 **B., Kimm, H., Pederson, T.L., Lipka, A.E., Bernacchi, C.J., et al.** (2023).
928 Reductions in leaf area index, pod production, seed size, and harvest index drive
929 yield loss to high temperatures in soybean. J Exp Bot **74**:1629-1641.
930 10.1093/jxb/erac503.

931 **Casal, J.J., and Questa, J.I.** (2018). Light and temperature cues: multitasking
932 receptors and transcriptional integrators. New Phytol **217**:1029-1034.
933 10.1111/nph.14890.

934 **Casal, J.J., and Balasubramanian, S.** (2019). Thermomorphogenesis. Annu Rev
935 Plant Biol **70**:321-346. 10.1146/annurev-arplant-050718-095919.

936 **Chow, B.Y., Helfer, A., Nusinow, D.A., and Kay, S.A.** (2012). ELF3 recruitment to
937 the PRR9 promoter requires other Evening Complex members in the Arabidopsis
938 circadian clock. Plant Signal Behav **7**:170-173. 10.4161/psb.18766.

939 **Chung, B.Y.W., Balcerowicz, M., Di Antonio, M., Jaeger, K.E., Geng, F.,**
940 **Franaszek, K., Marriott, P., Brierley, I., Firth, A.E., and Wigge, P.A.** (2020). An

941 RNA thermoswitch regulates daytime growth in Arabidopsis. Nat Plants **6**:522-532.
942 10.1038/s41477-020-0633-3.

943 **Crawford, A.J., McLachlan, D.H., Hetherington, A.M., and Franklin, K.A.** (2012).
944 High temperature exposure increases plant cooling capacity. Curr Biol **22**:R396-397.
945 10.1016/j.cub.2012.03.044.

946 **Crocco, C.D., Locascio, A., Escudero, C.M., Alabadi, D., Blazquez, M.A., and**
947 **Botto, J.F.** (2015). The transcriptional regulator BBX24 impairs DELLA activity to
948 promote shade avoidance in Arabidopsis thaliana. Nat Commun **6**:6202.
949 10.1038/ncomms7202.

950 **de Lucas, M., Daviere, J.M., Rodriguez-Falcon, M., Pontin, M., Iglesias-Pedraz,**
951 **J.M., Lorrain, S., Fankhauser, C., Blazquez, M.A., Titarenko, E., and Prat, S.**
952 (2008). A molecular framework for light and gibberellin control of cell elongation.
953 Nature **451**:480-484. 10.1038/nature06520.

954 **Delker, C., Quint, M., and Wigge, P.A.** (2022). Recent advances in understanding
955 thermomorphogenesis signaling. Curr Opin Plant Biol **68**:102231.
956 10.1016/j.pbi.2022.102231.

957 **Ding, L., Wang, S., Song, Z.T., Jiang, Y., Han, J.J., Lu, S.J., Li, L., and Liu, J.X.**
958 (2018). Two B-Box Domain Proteins, BBX18 and BBX23, Interact with ELF3 and
959 Regulate Thermomorphogenesis in Arabidopsis. Cell Rep **25**:1718-1728 e1714.
960 10.1016/j.celrep.2018.10.060.

961 **Favero, D.S., Kawamura, A., Shibata, M., Takebayashi, A., Jung, J.H., Suzuki,**
962 **T., Jaeger, K.E., Ishida, T., Iwase, A., Wigge, P.A., et al.** (2020). AT-Hook
963 Transcription Factors Restrict Petiole Growth by Antagonizing PIFs. Curr Biol
964 **30**:1454-1466 e1456. 10.1016/j.cub.2020.02.017.

965 **Fiorucci, A.S., Galvão, V.C., Ince, Y., Boccaccini, A., Goyal, A., Allenbach**
966 **Petrolati, L., Trevisan, M., and Fankhauser, C.** (2020). PHYTOCHROME
967 INTERACTING FACTOR 7 is important for early responses to elevated temperature
968 in Arabidopsis seedlings. New Phytol **226**:50-58. 10.1111/nph.16316.

969 **Franklin, K.A., Toledo-Ortiz, G., Pyott, D.E., and Halliday, K.J.** (2014). Interaction
970 of light and temperature signalling. J Exp Bot **65**:2859-2871. 10.1093/jxb/eru059.

971 **Franklin, K.A., Lee, S.H., Patel, D., Kumar, S.V., Spartz, A.K., Gu, C., Ye, S., Yu,**
972 **P., Breen, G., Cohen, J.D., et al.** (2011). Phytochrome-interacting factor 4 (PIF4)
973 regulates auxin biosynthesis at high temperature. Proc Natl Acad Sci U S A
974 **108**:20231-20235. 10.1073/pnas.1110682108.

975 **Gangappa, S.N., and Botto, J.F.** (2014). The BBX family of plant transcription
976 factors. Trends in Plant Science **19**:460-470. 10.1016/j.tplants.2014.01.010.

977 **Gangappa, S.N., and Kumar, S.V.** (2017). DET1 and HY5 Control PIF4-Mediated
978 Thermosensory Elongation Growth through Distinct Mechanisms. Cell Rep **18**:344-
979 351. 10.1016/j.celrep.2016.12.046.

980 **Gangappa, S.N., Berriri, S., and Kumar, S.V.** (2017). PIF4 Coordinates
981 Thermosensory Growth and Immunity in Arabidopsis. Curr Biol **27**:243-249.
982 10.1016/j.cub.2016.11.012.

983 **Gangappa, S.N., Crocco, C.D., Johansson, H., Datta, S., Hettiarachchi, C.,**
984 **Holm, M., and Botto, J.F.** (2013). The Arabidopsis B-BOX protein BBX25 interacts
985 with HY5, negatively regulating BBX22 expression to suppress seedling
986 photomorphogenesis. Plant Cell **25**:1243-1257. 10.1105/tpc.113.109751.

987 **Gray, W.M., Ostin, A., Sandberg, G., Romano, C.P., and Estelle, M.** (1998). High
988 temperature promotes auxin-mediated hypocotyl elongation in Arabidopsis. Proc
989 Natl Acad Sci U S A **95**:7197-7202. 10.1073/pnas.95.12.7197.

990 **Helfer, A., Nusinow, D.A., Chow, B.Y., Gehrke, A.R., Bulyk, M.L., and Kay, S.A.**
991 (2011). LUX ARRHYTHMO encodes a nighttime repressor of circadian gene
992 expression in the Arabidopsis core clock. Curr Biol **21**:126-133.
993 10.1016/j.cub.2010.12.021.

994 **Huang, Y., Xiong, H., Xie, Y., Lyu, S., Miao, T., Li, T., Lyu, G., and Li, S.** (2022).
995 BBX24 Interacts with DELLA to Regulate UV-B-Induced Photomorphogenesis in
996 Arabidopsis thaliana. Int J Mol Sci **23**10.3390/ijms23137386.

997 **Huq, E., and Quail, P.H.** (2002). PIF4, a phytochrome-interacting bHLH factor,
998 functions as a negative regulator of phytochrome B signaling in Arabidopsis. EMBO
999 J **21**:2441-2450. 10.1093/emboj/21.10.2441.

1000 **Ibanez, C., Delker, C., Martinez, C., Burstenbinder, K., Janitza, P., Lippmann,**
1001 **R., Ludwig, W., Sun, H., James, G.V., Klecker, M., et al.** (2018). Brassinosteroids
1002 Dominate Hormonal Regulation of Plant Thermomorphogenesis via BZR1. Curr Biol
1003 **28**:303-310 e303. 10.1016/j.cub.2017.11.077.

1004 **Jiang, L., Wang, Y., Li, Q.F., Bjorn, L.O., He, J.X., and Li, S.S.** (2012). Arabidopsis
1005 STO/BBX24 negatively regulates UV-B signaling by interacting with COP1 and
1006 repressing HY5 transcriptional activity. Cell Res **22**:1046-1057. 10.1038/cr.2012.34.

1007 **Job, N., Yadukrishnan, P., Bursch, K., Datta, S., and Johansson, H.** (2018). Two
1008 B-Box Proteins Regulate Photomorphogenesis by Oppositely Modulating HY5
1009 through their Diverse C-Terminal Domains. Plant Physiol **176**:2963-2976.
1010 10.1104/pp.17.00856.

1011 **Jung, J.H., Barbosa, A.D., Hutin, S., Kumita, J.R., Gao, M., Derwort, D., Silva,**
1012 **C.S., Lai, X., Pierre, E., Geng, F., et al.** (2020). A prion-like domain in ELF3
1013 functions as a thermosensor in Arabidopsis. Nature **585**:256-260. 10.1038/s41586-
1014 020-2644-7.

1015 **Jung, J.H., Domijan, M., Klose, C., Biswas, S., Ezer, D., Gao, M.J., Khattak, A.K.,**
1016 **Box, M.S., Charoensawan, V., Cortijo, S., et al.** (2016). Phytochromes function as
1017 thermosensors in. Science **354**:886-889. 10.1126/science.aaf6005.

1018 **Khanna, R., Kronmiller, B., Maszle, D.R., Coupland, G., Holm, M., Mizuno, T.,**
1019 **and Wu, S.H.** (2009). The Arabidopsis B-box zinc finger family. Plant Cell **21**:3416-
1020 3420. 10.1105/tpc.109.069088.

1021 **Koester, R.P., Skoneczka, J.A., Cary, T.R., Diers, B.W., and Ainsworth, E.A.**
1022 (2014). Historical gains in soybean (Glycine max Merr.) seed yield are driven by
1023 linear increases in light interception, energy conversion, and partitioning efficiencies.
1024 J Exp Bot **65**:3311-3321. 10.1093/jxb/eru187.

1025 **Koini, M.A., Alvey, L., Allen, T., Tilley, C.A., Harberd, N.P., Whitelam, G.C., and**
1026 **Franklin, K.A.** (2009). High temperature-mediated adaptations in plant architecture
1027 require the bHLH transcription factor PIF4. Curr Biol **19**:408-413.
1028 10.1016/j.cub.2009.01.046.

1029 **Krahmer, J., and Fankhauser, C.** (2023). Environmental Control of Hypocotyl
1030 Elongation. Annu Rev Plant Biol 10.1146/annurev-arplant-062923-023852.

1031 **Kumar, S.V., Lucyshyn, D., Jaeger, K.E., Alos, E., Alvey, E., Harberd, N.P., and**
1032 **Wigge, P.A.** (2012). Transcription factor PIF4 controls the thermosensory activation
1033 of flowering. Nature **484**:242-245. 10.1038/nature10928.

1034 **Lee, S., Paik, I., and Huq, E.** (2020). SPAs promote thermomorphogenesis by
1035 regulating the phyB-PIF4 module in Arabidopsis. Development
1036 **147**10.1242/dev.189233.

1037 **Legris, M., Ince, Y.C., and Fankhauser, C.** (2019). Molecular mechanisms
1038 underlying phytochrome-controlled morphogenesis in plants. Nat Commun **10**:5219.
1039 10.1038/s41467-019-13045-0.

1040 **Legris, M., Klose, C., Burgie, E.S., Rojas, C.C., Neme, M., Hiltbrunner, A.,**
1041 **Wigge, P.A., Schafer, E., Vierstra, R.D., and Casal, J.J.** (2016). Phytochrome B
1042 integrates light and temperature signals in Arabidopsis. Science **354**:897-900.
1043 10.1126/science.aaf5656.

1044 **Li, F., Sun, J., Wang, D., Bai, S., Clarke, A.K., and Holm, M.** (2014). The B-box
1045 family gene STO (BBX24) in Arabidopsis thaliana regulates flowering time in
1046 different pathways. PLoS One **9**:e87544. 10.1371/journal.pone.0087544.

1047 **Li, K.L., Yu, R.B., Fan, L.M., Wei, N., Chen, H.D., and Deng, X.W.** (2016). DELLA-
1048 mediated PIF degradation contributes to coordination of light and gibberellin
1049 signalling in. Nature Communications **7**ARTN 11868

1050 10.1038/ncomms11868.

1051 **Lippmann, R., Babben, S., Menger, A., Delker, C., and Quint, M.** (2019).
1052 Development of Wild and Cultivated Plants under Global Warming Conditions. Curr
1053 Biol **29**:R1326-R1338. 10.1016/j.cub.2019.10.016.

1054 **Lorrain, S., Allen, T., Duek, P.D., Whitelam, G.C., and Fankhauser, C.** (2008).
1055 Phytochrome-mediated inhibition of shade avoidance involves degradation of
1056 growth-promoting bHLH transcription factors. Plant J **53**:312-323. 10.1111/j.1365-
1057 313X.2007.03341.x.

1058 **Ma, D., Li, X., Guo, Y., Chu, J., Fang, S., Yan, C., Noel, J.P., and Liu, H.** (2016).
1059 Cryptochrome 1 interacts with PIF4 to regulate high temperature-mediated hypocotyl
1060 elongation in response to blue light. Proc Natl Acad Sci U S A **113**:224-229.
1061 10.1073/pnas.1511437113.

1062 **Nakamura, S., Mano, S., Tanaka, Y., Ohnishi, M., Nakamori, C., Araki, M., Niwa,**
1063 **T., Nishimura, M., Kaminaka, H., Nakagawa, T., et al.** (2010). Gateway Binary
1064 Vectors with the Bialaphos Resistance Gene,

1065 , as a Selection Marker for Plant Transformation. Biosci Biotech Bioch **74**:1315-1319.
1066 10.1271/bbb.100184.

1067 **Nieto, C., Lopez-Salmeron, V., Daviere, J.M., and Prat, S.** (2015). ELF3-PIF4
1068 interaction regulates plant growth independently of the Evening Complex. Curr Biol
1069 **25**:187-193. 10.1016/j.cub.2014.10.070.

1070 **Nusinow, D.A., Helfer, A., Hamilton, E.E., King, J.J., Imaizumi, T., Schultz, T.F.,**
1071 **Farre, E.M., and Kay, S.A.** (2011). The ELF4-ELF3-LUX complex links the circadian
1072 clock to diurnal control of hypocotyl growth. Nature **475**:398-402.
1073 10.1038/nature10182.

1074 **Oh, E., Zhu, J.Y., and Wang, Z.Y.** (2012). Interaction between BZR1 and PIF4
1075 integrates brassinosteroid and environmental responses. Nat Cell Biol **14**:802-809.
1076 10.1038/ncb2545.

1077 **Park, Y.J., Lee, H.J., Ha, J.H., Kim, J.Y., and Park, C.M.** (2017). COP1 conveys
1078 warm temperature information to hypocotyl thermomorphogenesis. New Phytol
1079 **215**:269-280. 10.1111/nph.14581.

1080 **Peng, S., Huang, J., Sheehy, J.E., Laza, R.C., Visperas, R.M., Zhong, X.,**
1081 **Centeno, G.S., Khush, G.S., and Cassman, K.G.** (2004). Rice yields decline with
1082 higher night temperature from global warming. Proc Natl Acad Sci U S A **101**:9971-
1083 9975. 10.1073/pnas.0403720101.

1084 **Podolec, R., Wagnon, T.B., Leonardelli, M., Johansson, H., and Ulm, R.** (2022).
1085 Arabidopsis B-box transcription factors BBX20-22 promote UVR8 photoreceptor-
1086 mediated UV-B responses. Plant J **111**:422-439. 10.1111/tpj.15806.

1087 **Qiu, Y., Li, M., Kim, R.J., Moore, C.M., and Chen, M.** (2019). Daytime temperature
1088 is sensed by phytochrome B in Arabidopsis through a transcriptional activator
1089 HEMERA. Nat Commun **10**:140. 10.1038/s41467-018-08059-z.

1090 **Qiu, Y., Pasoreck, E.K., Yoo, C.Y., He, J., Wang, H., Bajracharya, A., Li, M.,**
1091 **Larsen, H.D., Cheung, S., and Chen, M.** (2021). RCB initiates Arabidopsis
1092 thermomorphogenesis by stabilizing the thermoregulator PIF4 in the daytime. Nat
1093 Commun **12**:2042. 10.1038/s41467-021-22313-x.

1094 **Quint, M., Delker, C., Franklin, K.A., Wigge, P.A., Halliday, K.J., and van Zanten,**
1095 **M.** (2016). Molecular and genetic control of plant thermomorphogenesis. Nat Plants
1096 **2**:15190. 10.1038/nplants.2015.190.

1097 **Quint, M., Delker, C., Balasubramanian, S., Balcerowicz, M., Casal, J.J.,**
1098 **Castroverde, C.D.M., Chen, M., Chen, X., De Smet, I., Fankhauser, C., et al.**
1099 (2023). 25 Years of thermomorphogenesis research: milestones and perspectives.
1100 Trends Plant Sci **28**:1098-1100. 10.1016/j.tplants.2023.07.001.

1101 **Saura-Sanchez, M., Chiriotto, T.S., Cascales, J., Gomez-Ocampo, G.,**
1102 **Hernandez-Garcia, J., Li, Z., Pruneda-Paz, J.L., Blazquez, M.A., and Botto, J.F.**
1103 (2023). BBX24 Interacts with JAZ3 to Promote Growth by Reducing DELLA Activity
1104 in Shade Avoidance. Plant Cell Physiol **64**:474-485. 10.1093/pcp/pcad011.

1105 **Silva, C.S., Nayak, A., Lai, X., Hutin, S., Hugouvieux, V., Jung, J.H., Lopez-**
1106 **Vidriero, I., Franco-Zorrilla, J.M., Panigrahi, K.C.S., Nanao, M.H., et al.** (2020).
1107 Molecular mechanisms of Evening Complex activity in Arabidopsis. Proc Natl Acad
1108 Sci U S A **117**:6901-6909. 10.1073/pnas.1920972117.

Song, Z.Q., Bian, Y.T., Liu, J.J., Sun, Y., and Xu, D. (2020). B-box proteins: Pivotal players in light-mediated development in plants. Journal of Integrative Plant Biology **62**:1293-1309. 10.1111/jipb.12935.

Stavang, J.A., Gallego-Bartolome, J., Gomez, M.D., Yoshida, S., Asami, T., Olsen, J.E., Garcia-Martinez, J.L., Alabadi, D., and Blazquez, M.A. (2009). Hormonal regulation of temperature-induced growth in Arabidopsis. Plant J **60**:589-601. 10.1111/j.1365-313X.2009.03983.x.

Sun, J., Qi, L., Li, Y., Chu, J., and Li, C. (2012). PIF4-mediated activation of YUCCA8 expression integrates temperature into the auxin pathway in regulating arabidopsis hypocotyl growth. PLoS Genet **8**:e1002594. 10.1371/journal.pgen.1002594.

Tan, W., Chen, J., Yue, X., Chai, S., Liu, W., Li, C., Yang, F., Gao, Y., Gutiérrez Rodríguez, L., Resco de Dios, V., et al. (2023a). The heat response regulators HSFA1s promote Arabidopsis thermomorphogenesis via stabilizing PIF4 during the day. Sci Adv **9**:eadh1738. 10.1126/sciadv.adh1738.

Tan, W., Chen, J., Yue, X., Chai, S., Liu, W., Li, C., Yang, F., Gao, Y., Gutierrez Rodriguez, L., Resco de Dios, V., et al. (2023b). The heat response regulators HSFA1s promote Arabidopsis thermomorphogenesis via stabilizing PIF4 during the day. Sci Adv **9**:eadh1738. 10.1126/sciadv.adh1738.

Tripathi, P., Carvallo, M., Hamilton, E.E., Preuss, S., and Kay, S.A. (2017). Arabidopsis B-BOX32 interacts with CONSTANS-LIKE3 to regulate flowering. Proc Natl Acad Sci U S A **114**:172-177. 10.1073/pnas.1616459114.

Vaishak, K.P., Yadukrishnan, P., Bakshi, S., Kushwaha, A.K., Ramachandran, H., Job, N., Babu, D., and Datta, S. (2019). The B-box bridge between light and hormones in plants. J Photoch Photobio B **191**:164-174. 10.1016/j.jphotobiol.2018.12.021.

Wang, C.Q., Guthrie, C., Sarmast, M.K., and Dehesh, K. (2014). BBX19 interacts with CONSTANS to repress FLOWERING LOCUS T transcription, defining a flowering time checkpoint in Arabidopsis. Plant Cell **26**:3589-3602. 10.1105/tpc.114.130252.

Xu, K., Huang, X., Wu, M., Wang, Y., Chang, Y., Liu, K., Zhang, J., Zhang, Y., Zhang, F., Yi, L., et al. (2014). A rapid, highly efficient and economical method of Agrobacterium-mediated in planta transient transformation in living onion epidermis. PLoS One **9**:e83556. 10.1371/journal.pone.0083556.

Yamaguchi, N., Winter, C.M., Wu, M.F., Kwon, C.S., William, D.A., and Wagner, D. (2014). PROTOCOLS: Chromatin Immunoprecipitation from Arabidopsis Tissues. Arabidopsis Book **12**:e0170. 10.1199/tab.0170.

Yuan, L., Yu, Y.J., Liu, M.M., Song, Y., Li, H.M., Sun, J.Q., Wang, Q., Xie, Q.G., Wang, L., and Xu, X.D. (2021). BBX19 fine-tunes the circadian rhythm by interacting with PSEUDO-RESPONSE REGULATOR proteins to facilitate their repressive effect on morning-phased clock genes. Plant Cell **33**:2602-2617. 10.1093/plcell/koab133.

Zhao, C., Liu, B., Piao, S., Wang, X., Lobell, D.B., Huang, Y., Huang, M., Yao, Y., Bassu, S., Ciais, P., et al. (2017). Temperature increase reduces global yields of major crops in four independent estimates. Proc Natl Acad Sci U S A **114**:9326-9331. 10.1073/pnas.1701762114.

Zhao, H., and Bao, Y. (2021). PIF4: Integrator of light and temperature cues in plant growth. Plant Sci **313**:111086. 10.1016/j.plantsci.2021.111086.

Zhao, X., Heng, Y., Wang, X., Deng, X.W., and Xu, D. (2020). A Positive Feedback Loop of BBX11-BBX21-HY5 Promotes Photomorphogenic Development in Arabidopsis. Plant Commun **1**:100045. 10.1016/j.xplc.2020.100045.

Zhou, Y., Park, S.-H., Soh, M.Y., and Chua, N.-H. (2021). Ubiquitin-specific proteases UBP12 and UBP13 promote shade avoidance response by enhancing PIF7 stability. Proceedings of the National Academy of Sciences **118**:e2103633118. doi:10.1073/pnas.210363311

FIGURES AND FIGURE LEGENDS

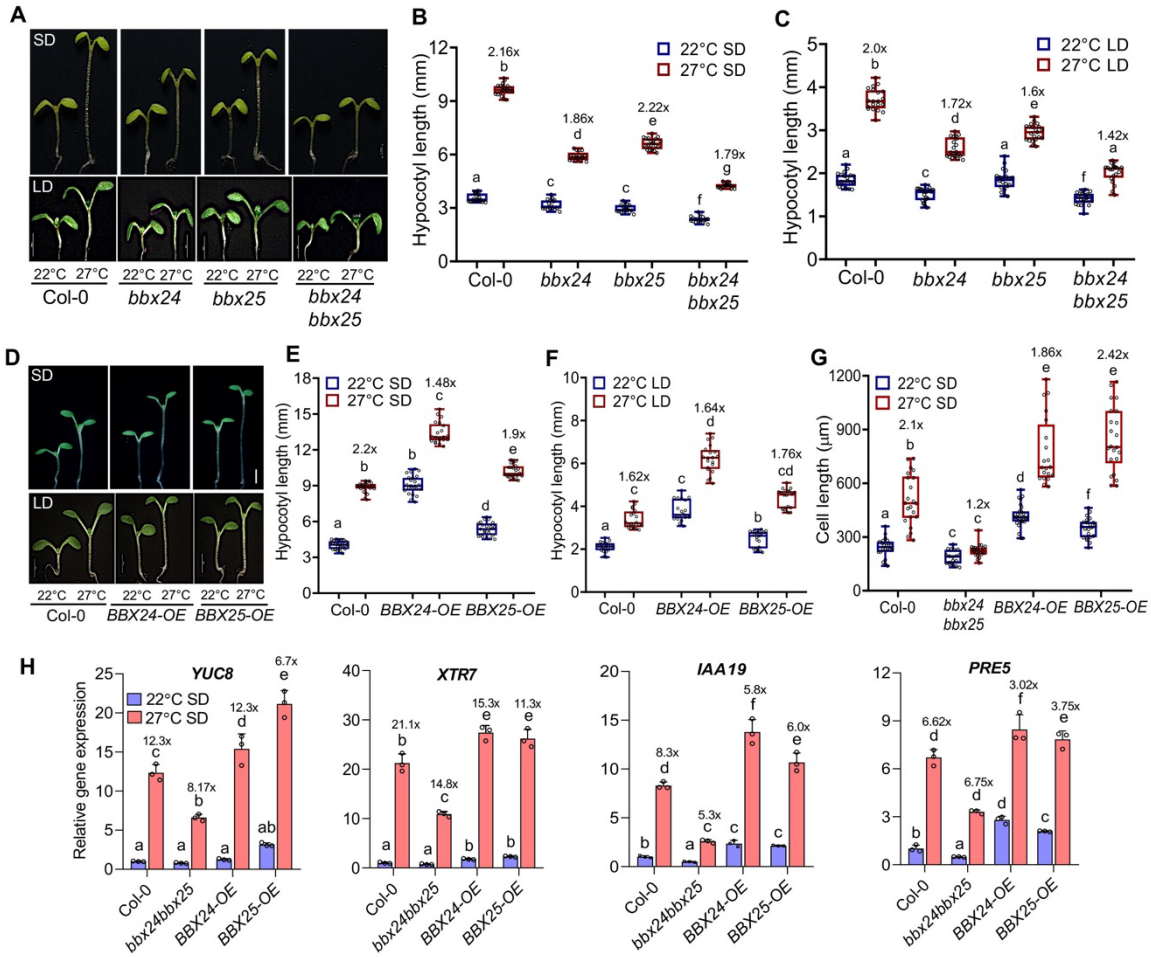

Figure 1. BBX24 and BBX25 promote thermosensory hypocotyl growth and gene expression.

(A) Representative images of six-day-old Col-0, *bbx24*, *bbx25*, and *bbx24bbx25* seedlings grown at 22°C and 27°C under short-day (SD, upper panel) and long-day (LD, lower panel) photoperiods.

(B-C) Hypocotyl length measurements (mean ± SD; n ≥ 20) of SD (**b**) and LD (**c**) grown seedlings that are shown in **A**.

(D) Representative seedling images of Col-0, *BBX24-OE*, and *BBX25-OE* lines (line #16) were grown at 22°C and 27°C for six days under SD (upper panel) and LD (lower panel) conditions.

(E and **F)** Hypocotyl length (mean ± SD; n ≥ 20) of SD (**E**) and LD (**F**) grown seedlings shown in (**D**).

(G) Cell length (mean ± SD; n ≥ 15) of hypocotyl epidermal cells from indicated genotypes grown at 22°C and 27°C for six days under SD.

(H) qRT-PCR analysis (mean ± SD of three biological replicates) showing relative transcript levels of thermoresponsive genes *YUC8*, *XTR7*, *IAA19* and *PRE5* in the

1204 indicated genotypes that were grown for six days at 22°C and 27°C under SD, and
1205 the samples were harvested at ZT23. *EF1α* was used as an internal control.
1206 In Figs. **B**, **C**, **E**-**G**, and **h**, different lowercase letters, shown above the bars, denote
1207 statistically significant differences between the samples (Two-way ANOVA followed
1208 by Tukey's post-hoc test, $p < 0.05$). Numbers indicate fold changes between 22°C
1209 and 27°C. All the experiments were repeated at least three times, and similar results
1210 were obtained. In Figure **A** and **D**, the scale bar represents 1 mm and 2 mm,
1211 respectively. All the experiments were repeated three times, and similar results were
1212 observed.
1213

1214

1215

1216

1217

1218

1219

1220

1221

1222

1223

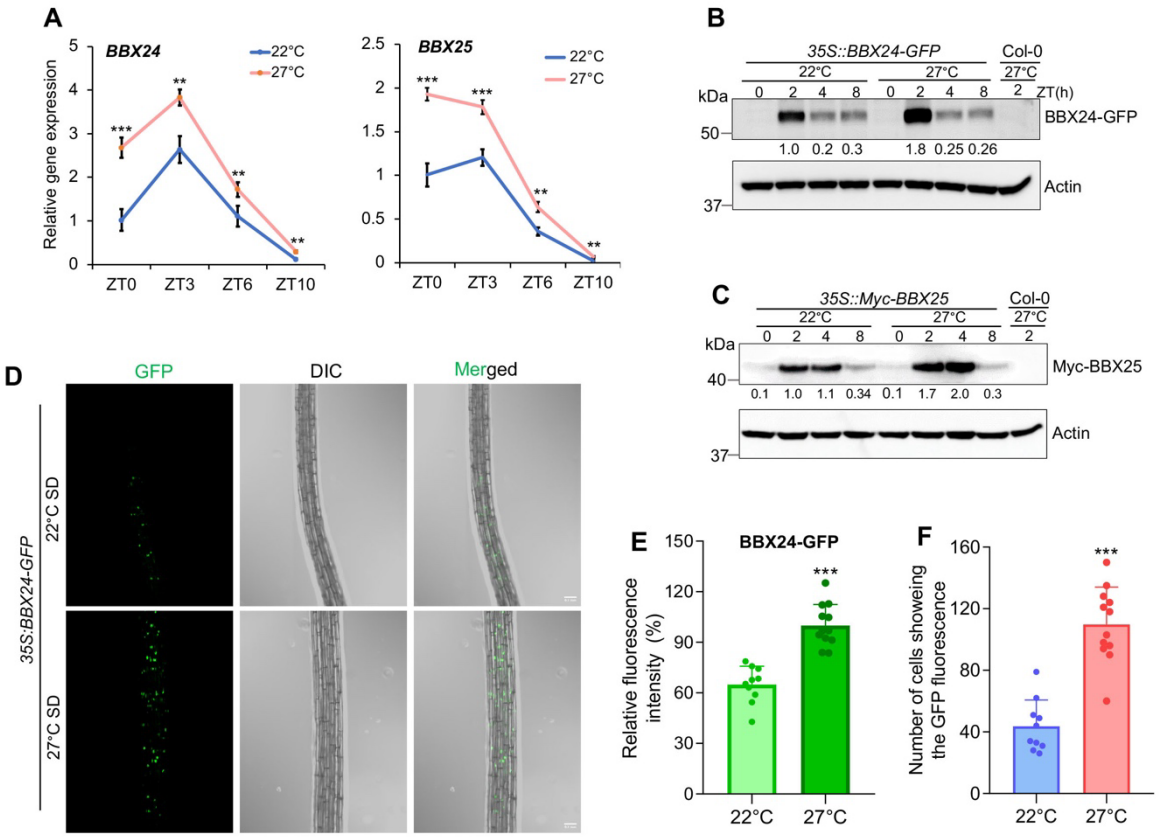

Figure 2. Warm temperatures promote BBX24/BBX25 transcript and protein accumulation.

(A) qRT-PCR analysis shows *BBX24* and *BBX25* expression in six-day-old Col-0 seedlings grown at 22°C and 27°C under SD conditions, and samples were collected at indicated time points. *EF1α* was used as a loading control, and the transcript level of each sample was normalized to Col-0 22°C ZT0 time point. Error bars depict the mean ± SD of three biological replicates. Asterisks denote statistically significant differences as determined by Student's t-test, **P<0.01, ***P<0.001.

(B) Immunoblots showing BBX24-GFP protein level in six-days-old *35S::BBX24-GFP* seedlings grown at 22°C and 27°C under SD photoperiod and samples were harvested at different time points as indicated.

(C) Immunoblot showing Myc-BBX25 protein status in six-days-old *35S::Myc-BBX25* seedlings grown at 22°C and 27°C under SD, and samples were harvested at different time points as indicated.

In Figure **B** and **C**, 27°C grown Col-0 seedlings harvested at ZT2 were used as a negative control. Actin served as a loading control and was used for normalization. Relative protein levels (shown underneath each immunoblot) were calculated by

1242 setting 22°C grown Col-0 ZT2 to 1. The experiments were repeated three times, and
1243 similar results were obtained.
1244 **(D-F)** Representative images (**D**), relative GFP fluorescence intensity (**E**) and
1245 number of cells showing the fluorescence (**F**) in hypocotyls of *35S:BBX24-GFP*
1246 transgenic seedlings grown for six days after germination at 22°C and 27°C under
1247 short-day conditions. At least ten seedlings have been captured for the GFP
1248 fluorescence. Asterisks denote statistically significant differences as determined by
1249 Student's t-test, ***P<0.001. All the experiments were repeated three times, and
1250 similar results were observed.
1251

1252

1253

1254

1255

1256

1257

1258

1259

1260

1261

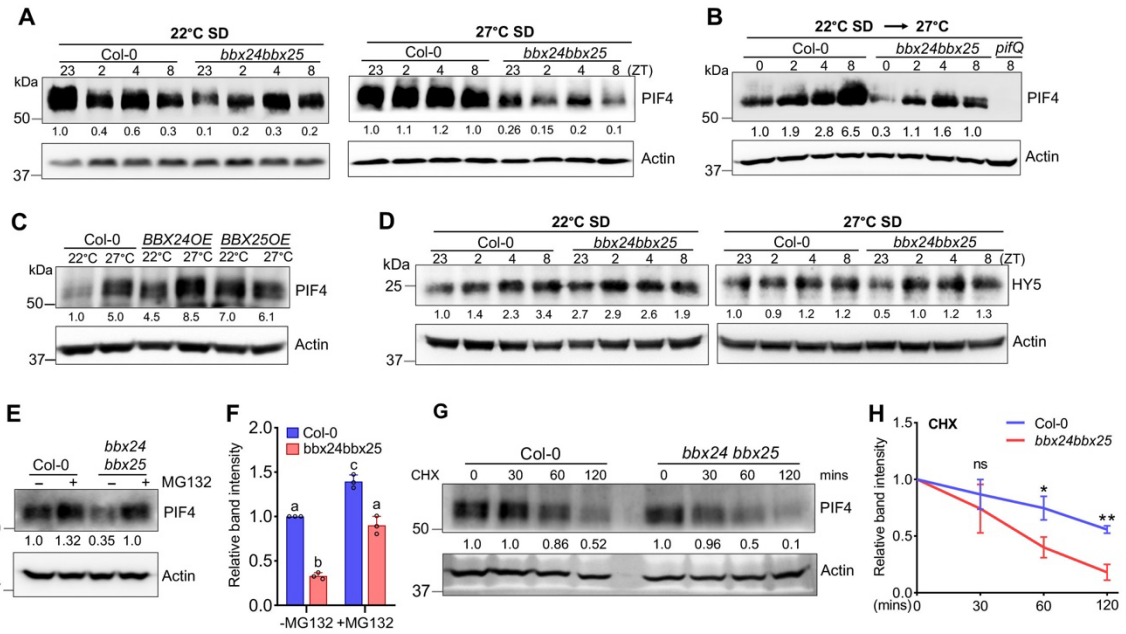

Figure 3. BBX24/BBX25 promotes the accumulation of PIF4 protein in response to warm temperatures.

(A) Immunoblot analysis of PIF4 protein levels in six-day-old Col-0 and *bbx24bbx25* seedlings grown diurnally at 22°C and 27°C under SD and samples were harvested at the indicated time (ZT) points.

(B) Immunoblot showing PIF4 protein levels in Col-0 and *bbx24bbx25* double mutant seedlings grown at 22°C SD for six days or 22°C SD grown seedlings exposed to 27°C for indicated time points. The *pifQ* mutant was used as a negative control.

(C) Immunoblot analysis of PIF4 protein level in six-day-old Col-0, *BBX24-OE*, and *BBX25-OE* seedlings grown at constant 22°C and 27°C under SD photoperiod, and tissue were harvested at ZT23.

(D) Immunoblot analysis of HY5 protein levels in six-day-old Col-0 and *bbx24bbx25* seedlings grown diurnally at 22°C and 27°C under SD and sampled at the indicated time (ZT) points.

(E and **F)** Immunoblot analysis (**E**) and relative band intensity of PIF4 protein levels (**F**) in six days-old 22°C SD grown Col-0 and *bbx24bbx25* double mutant seedlings shifted to 27°C for 24hrs with MG132 treatment for 16hrs before tissue harvest. Different lowercase letters, shown above the bars, denote statistically significant differences between the samples (Two-way ANOVA followed by Tukey's post-hoc test, $p < 0.05$).

(G and **H)** Western blot analysis (**G**) and relative band intensity of PIF4 protein degradation (**H**) in six-day-old 22°C SD grown Col-0 and *bbx24bbx25* double mutants seedlings treated with 50μM MG132 before being shifted to 27°C for 8hrs were washed five times and then transferred to liquid MS medium containing 200μM

1287 CHX following tissue harvest at the indicated time points. Asterisks represent
1288 statistically significant differences determined by the Student's t-test, *P<0.05,
1289 **P<0.01.
1290 Actin was used as a loading control in all the immunoblots. The relative PIF4 or HY5
1291 protein level normalized to actin was shown underneath the respective immunoblot.
1292 All the experiments were repeated three times, and similar results were observed.

1293

1294

1295

1296

1297

1298

1299

1300

1301

1302

1303

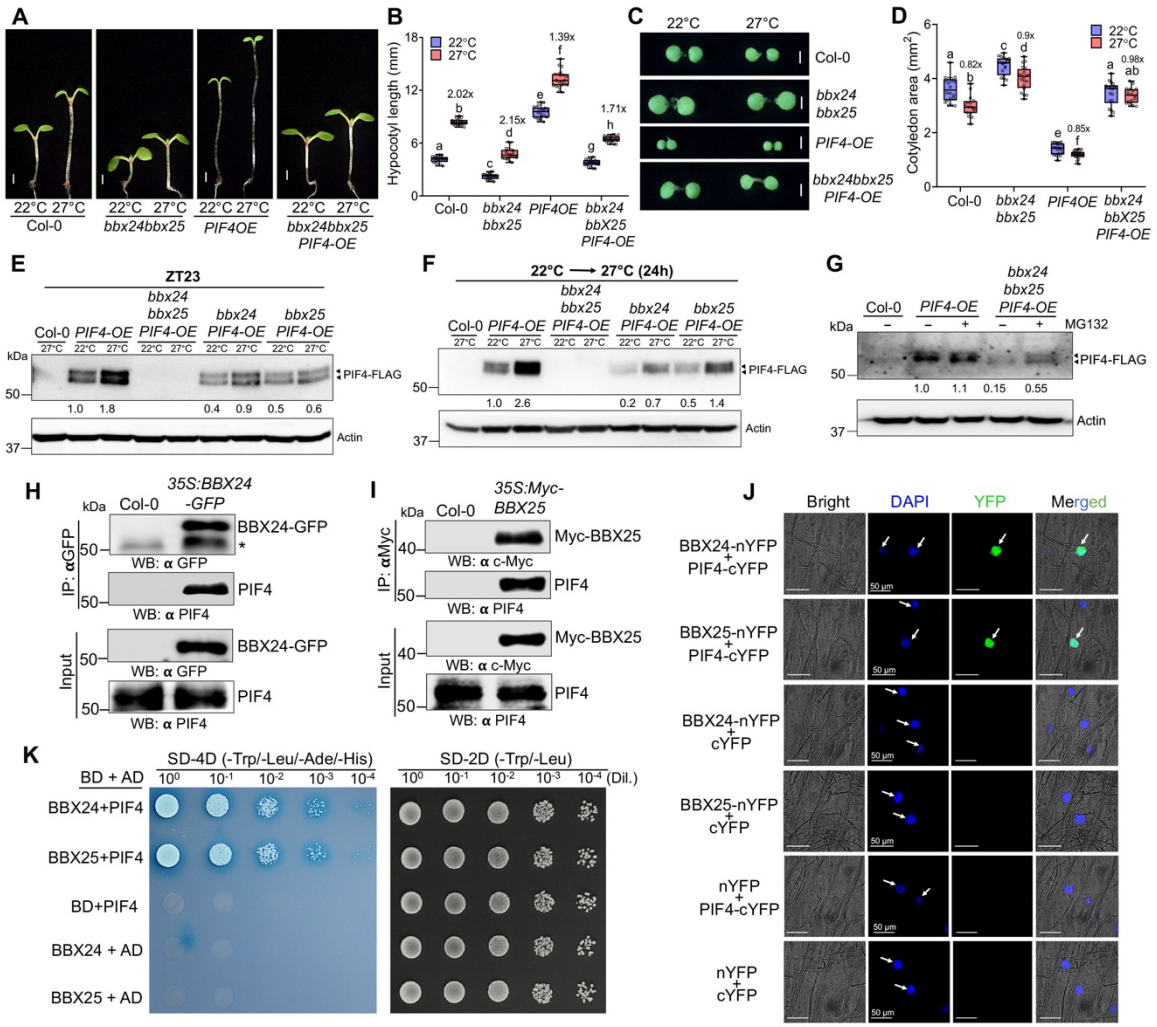

Figure 4. BBX24/BBX25 are essential for PIF4-mediated hypocotyl elongation in response to warm ambient temperatures.

(A and **B)** Representative seedlings images (a) and hypocotyl length (b) of six-days-old Col-0*, bbx24bbx25, PIF4-OE*, and *bbx24bbx25PIF4-OE* seedlings grown at 22°C and 27°C under SD. The data shown is mean ± SD (n ≥ 20) seedlings. The scale bar represents 1 mm.

(C and **D)** Representative cotyledon images (c) and cotyledon area (d) of six-day-old indicated genotypes grown at 22°C and 27°C under SD. The data shown is mean ± SD (n ≥ 20) of. The scale bar represents 1 mm. In Figs. b and d, different lowercase letters, shown above the bars, denote statistically significant differences between the samples (Two-way ANOVA followed by Tukey's post-hoc test, $p < 0.05$). Numbers indicate fold changes between 22°C and 27°C.

1317 **(E** and **F)** Immunoblot analysis of PIF4-FLAG protein levels in the indicated
1318 genotypes grown for six days at 22°C and 27°C, and samples were harvested at
1319 ZT23 (e), or 22°C SD grown five-day-old seedlings shifted to 27°C for 24h and
1320 sampled at ZT23 (f).
1321 **(G)** Immunoblot showing PIF4-FLAG protein levels in the indicated genotypes grown
1322 under 22°C SD for six days were shifted to 27°C for 24 h, followed by MG132
1323 treatment for 16 h before tissues were harvested. In Figs. **E-G**, Col-0 was used as a
1324 negative control. The relative PIF4 protein levels were normalized against Actin and
1325 are shown underneath each immunoblot. The normalized PIF4-FLAG protein levels
1326 in PIF4-OE at 22°C short day conditions were set to 1, and others were calculated
1327 as relative levels. We detected two bands of PIF4-FLAG, and the top band probably
1328 corresponds to the phosphorylated form of PIF4. Numbers indicate fold changes
1329 between 22°C and 27°C.
1330 **(H)** Immunoblots of coimmunoprecipitation assays showing BBX24 interacts with
1331 PIF4 in planta. Total protein from six-day-old Col-0 and *35S::BBX24-GFP* seedlings
1332 grown at 27°C, sampled at ZT2, were used, and BBX24-GFP was pulled down using
1333 anti-GFP antibody coupled to magnetic Dynabeads. BBX24-GFP and PIF4 from
1334 input and pulldown fractions were detected by immunoblot using anti-GFP and native
1335 anti-PIF4 antibodies. Asterisk denote a non-specific band.
1336 **(I)** Immunoblots of coimmunoprecipitation assay showing BBX25 interacts with PIF4
1337 in planta. Total protein from six-day-old Col-0 and *35S::Myc-BBX25* seedlings grown
1338 at 27°C, sampled at ZT2, were used, and Myc-BBX25 was immunoprecipitated using
1339 an anti-myc antibody coupled to magnetic Dynabeads. Myc-BBX25 and PIF4 from
1340 input and pulldown fractions were detected by immunoblotting using anti-Myc and
1341 native anti-PIF4 antibodies.
1342 **(J)** BiFC assays show the physical interaction of BBX24 and BBX25 with PIF4 in
1343 planta in onion epidermal cells. The adaxial epidermis of the onion bulb was co-
1344 infiltrated with nYFP, BBX24-nYFP, or BBX25-nYFP, and cYFP or PIF4-cYFP as
1345 indicated. Two days after incubation, onion peels were analysed for fluorescence in
1346 different combinations of co-infiltered samples.
1347 **(K)** BBX24 and BBX25 physically interact with PIF4 in yeast. Overnight grown
1348 cultures of Y2H Gold yeast strain containing different combinations of bait (pGBKT7,
1349 pGBKT7-BBX24, and pGBKT7-BBX25) and prey (pGADT7 and pGADT7-PIF4)
1350 constructs diluted to an OD_{600} of 0.5 with 4x serial dilutions were spotted on double
1351 and quadruple dropout medium supplemented with X-alpha-gal. Pictures were taken
1352 after 72 h of incubation at 30°C. The experiments were repeated at least three times,
1353 and similar results were obtained. All the interactions were repeated three times, and
1354 similar results were observed.

1355

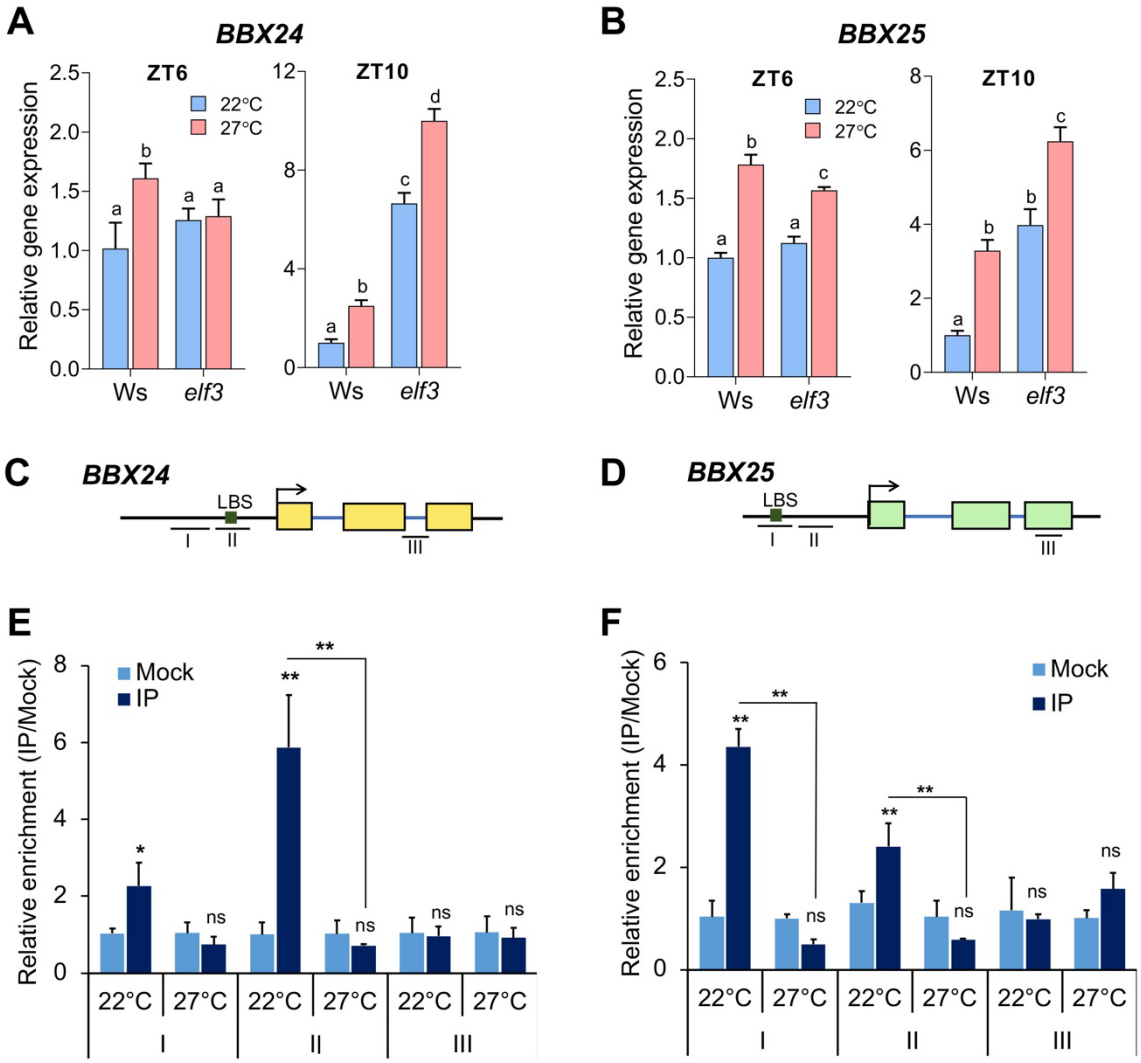

Figure 5. ELF3 represses *BBX24*/*BBX25* transcription during dawn while warm temperature dampens it.

(A and **B)** qRT-PCR analysis showing relative transcript levels of *BBX24* and *BBX25* in six-day-old seedlings of Ws and *elf3* grown at constant 22°C and 27°C SD conditions, sampled at ZT6 and ZT10. The expression level of each sample was normalized to Ws at 22°C of the respective time point, *and EF1α* was used as an internal control. The data shown is the mean ± SD, with Error bars depicting SD (n=3 biological replicates).

(C and **D)** Schematic representation of *BBX24* and *BBX25* promoters depicting LUX binding sites and the exact position of each PCR fragment used for analysis.

(E and **F)** ChIP-qPCR assay showing ELF3 enrichment onto *BBX24* and *BBX25* promoters in vivo. Six-day-old seedlings of *35S::ELF3-YFP* (*elf3-4*) grown at 22°C and 27°C SD conditions were sampled at ZT10 for cross-linking. For each amplicon, fold enrichment was calculated as a ratio between anti-GFP and mock (pre-immune

1371 serum). Genomic fragment towards the *3'UTR* of *BBX24* and *BBX25* was used as
1372 a negative control. The data shown is the (mean ± SD, n=2, two biological replicates.
1373 The experiment was repeated twice, and similar results were seen. Asterisks denote
1374 statistically significant differences as determined by Student's t-test, *P<0.05,
1375 **P<0.01.

1376

1377

1378

1379

1380

1381

1382

1383

1384

1385

1386

1387

1388

1389

1390

1391

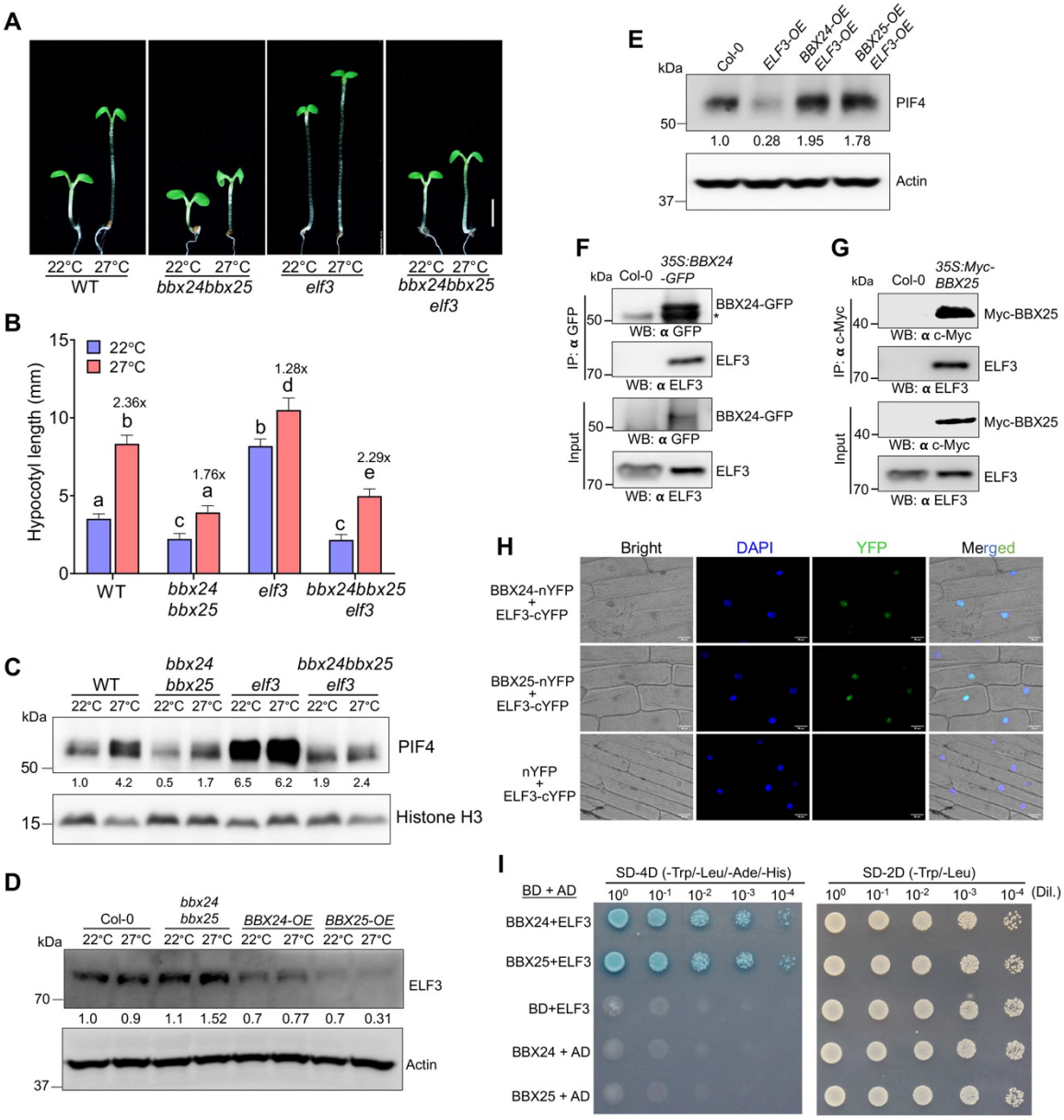

Figure 6. BBX24/BBX25 antagonizes ELF3 to promote PIF4-mediated thermosensory growth.

(A and **B)** Representative seedling images and hypocotyl length of six-day-old segregated WT (Col-0xWs), *bbx24bbx25*, *elf3* and *bbx24bbx25elf3* seedlings grown at 22°C and 27°C under SD. The scale bar = 2 mm. In Figure b, different lowercase letters, shown above the bars, denote statistically significant differences between the samples (Two-way ANOVA followed by Tukey's post-hoc test, $p < 0.05$). Numbers indicate fold changes between 22°C and 27°C.

1401 **(C)** Immunoblots showing PIF4 protein levels in WT (Col-0xWs), *bbx24bbx25*, *elf3*
1402 and *bbx24bbx25elf3* seedlings grown at 22°C for six days or transferred to 27°C for
1403 24 hours and harvested at ZT23. Histone H3 was used as a loading control, and the
1404 relative levels of PIF4 protein normalized to Histone H3 are shown underneath each
1405 immunoblot.
1406 **(D)** Immunoblot showing ELF3 protein levels in six-day-old Col-0, *bbx24bbx25*,
1407 *BBX24-OE* and BBX25-OE seedlings grown at constant 22°C and 27°C under short-
1408 day conditions. Actin was used as a loading control, and the relative ELF3 protein
1409 level was calculated against Col-0 at 22°C SD.
1410 **(E)** Immunoblot analysis of PIF4 protein levels of the indicated genotypes was
1411 shifted to 27°C for 24 hours after growing for five days at 22°C SD conditions. Actin
1412 was used as a loading control, and the relative PIF4 protein levels shown underneath
1413 the immunoblot were calculated against Col-0.
1414 **(F** and **G)** Co-immunoprecipitation assay showing in vivo protein-protein interactions
1415 between BBX24-ELF3 and BBX25-ELF3. Total protein from six-day-old Col-0,
1416 *35S:BBX24-GFP* and *35S:Myc-BBX25* seedlings grown at 22°C SD, harvested at
1417 ZT8, were used. The BBX24-GFP and BBX25-Myc proteins were pulled down using
1418 anti-GFP and anti-Myc antibodies coupled to magnetic Dynabeads. In the input and
1419 immunoprecipitated protein complex, ELF3 was detected using native anti-ELF3
1420 antibodies. Similarly, all the proteins were detected using respective antibodies in
1421 the input and immunoprecipitated fractions. Asterisk denote a non-specific band.
1422 **(H)** BiFC assays show the physical association of BBX24 and BBX25 with ELF3 in
1423 onion epidermal cells. The adaxial epidermis of the onion bulb was co-infiltrated with
1424 nYFP, BBX24-nYFP or BBX25-nYFP with cYFP or ELF3-cYFP, as indicated. After
1425 two days of incubation, onion peels were observed for fluorescence under a
1426 microscope in different co-infiltrate samples. Scale bar = 50 μm.
1427 **(I)** Yeast two-hybrid assay showing BBX24 and BBX25 physical interaction with
1428 ELF3 in yeast. Y2H Gold strain harbouring different combinations of bait (pGBKT7,
1429 pGBKT7-BBX24, and pGBKT7-BBX25) and prey (pGADT7 and pGADT7-ELF3)
1430 constructs were grown overnight to an OD_{600} of 0.5 with 4x serial dilutions were
1431 dropped on double and quadruple dropout medium supplemented with X-alpha-gal.
1432 Pictures were captured after incubating the plates for three days at 30°C. The
1433 experiments were repeated at least three times, and similar results were obtained.
1434
1435
1436
1437
1438
1439
1440

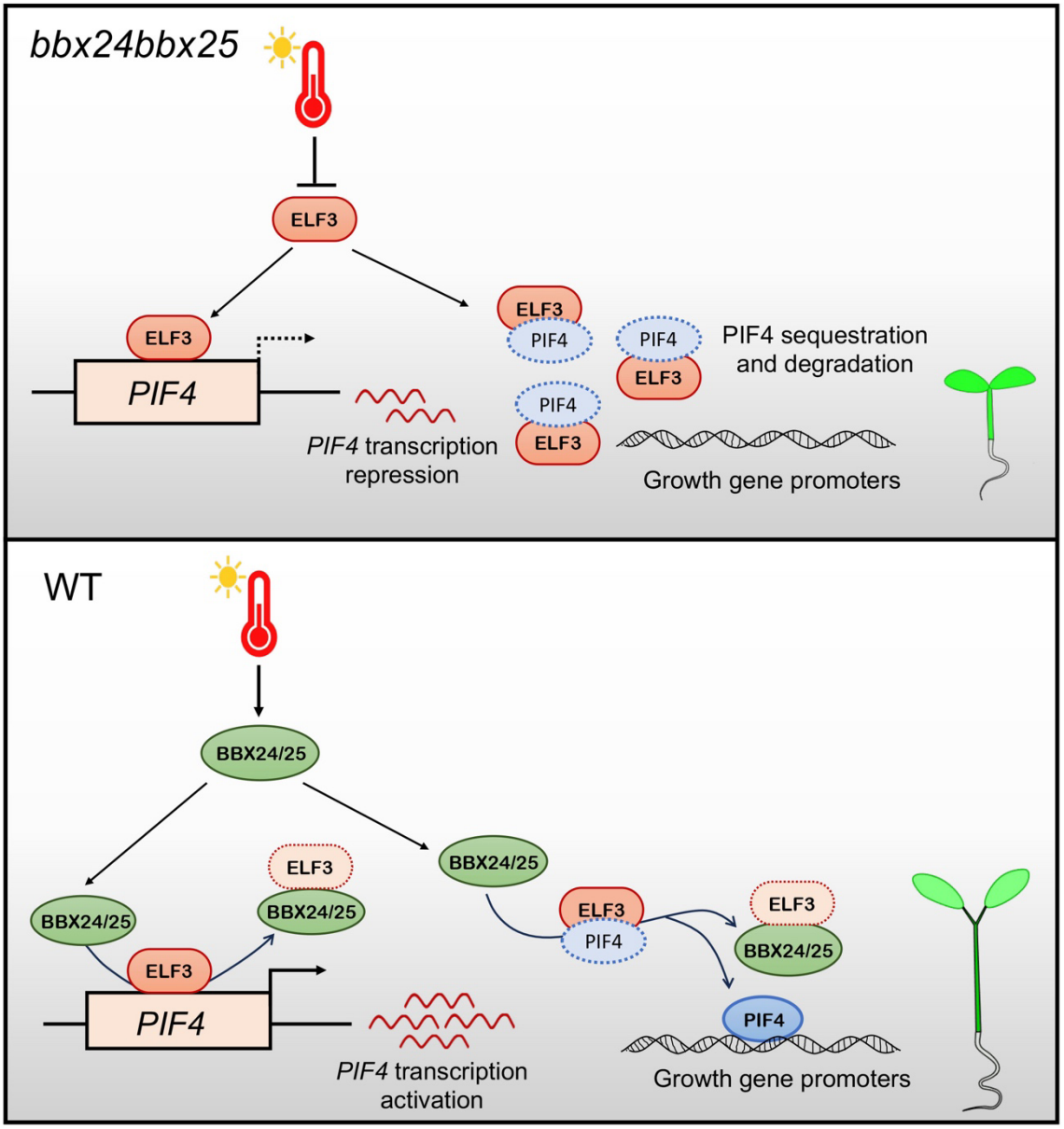

Figure 7. The molecular model depicting BBX24/BBX25-mediated regulation of thermosensory growth.

The model elucidates the molecular mechanism by which BBX24/BBX25 promotes thermosensory growth in Arabidopsis. In the absence of BBX24/BBX25, ELF3 exerts a robust inhibitory effect on PIF4 at the transcriptional and protein activity levels, resulting in compromised thermosensory responses. However, in the presence of BBX24/BBX25, they antagonize ELF3, relieving its inhibitory effect on PIF4, resulting in enhanced PIF4 function, and promoting warm temperature-mediated growth.

1451